

 Open access • Posted Content • DOI:10.1101/2021.04.02.438227

## Inability to switch from ARID1A-BAF to ARID1B-BAF impairs exit from pluripotency and commitment towards neural crest differentiation in ARID1B-related neurodevelopmental disorders — [Source link](#)

Luca Pagliaroli, Patrizia Porazzi, Alyxandra T. Curtis, Harald Mikkers ...+8 more authors

**Institutions:** Thomas Jefferson University, Leiden University Medical Center, Wistar Institute

**Published on:** 02 Apr 2021 - bioRxiv (Cold Spring Harbor Laboratory)

**Topics:** Cellular differentiation, SOX2, Cranial neural crest, Homeobox protein NANOG and Neural crest

Related papers:

- [Inability to switch from ARID1A-BAF to ARID1B-BAF impairs exit from pluripotency and commitment towards neural crest formation in ARID1B-related neurodevelopmental disorders.](#)
- [ARID4B is critical for mouse embryonic stem cell differentiation towards mesoderm and endoderm, linking epigenetics to pluripotency exit](#)
- [Chromatin remodeling mediated by ARID1A is indispensable for normal hematopoiesis in mice.](#)
- [Arid1a-Plagl1-Hh signaling is indispensable for differentiation-associated cell cycle arrest of tooth root progenitors.](#)
- [Arid4b physically interacts with Tfap2c in mouse embryonic stem cells.](#)

Share this paper:    

View more about this paper here: <https://typeset.io/papers/inability-to-switch-from-arid1a-baf-to-arid1b-baf-impairs-3htgaauk0i>

1 **Inability to switch from ARID1A-BAF to ARID1B-BAF impairs exit from pluripotency and commitment**  
2 **towards neural crest differentiation in ARID1B-related neurodevelopmental disorders**

3  
4 Luca Pagliaroli<sup>1</sup>, Patrizia Porazzi<sup>2</sup>, Alyxandra T. Curtis<sup>1</sup>, Harald M.M. Mikkers<sup>3</sup>, Christian Freund<sup>4</sup>, Lucia  
5 Daxinger<sup>5</sup>, Sandra Deliard<sup>6</sup>, Sarah A. Welsh<sup>6</sup>, Connor A. Ott<sup>1</sup>, Bruno Calabretta<sup>2</sup>, Gijs W.E. Santen<sup>\*7</sup>, and  
6 Marco Trizzino<sup>\*1,8</sup>

7  
8 \* = Co-Senior authors

9 1) Department of Biochemistry and Molecular Biology, Sidney Kimmel Medical College, Thomas Jefferson University,  
10 Philadelphia, PA

11 2) Department of Cancer Biology, Sidney Kimmel Medical College, Thomas Jefferson University, Philadelphia, PA

12 3) Department of Cell & Chemical Biology, Leiden University Medical Center, Leiden, The Netherlands

13 4) LUMC hiPSC Hotel, Dept. Anatomy & Embryology, Leiden University Medical Center, Leiden, The Netherlands

14 5) Department of Human Genetics, Leiden University Medical Center (LUMC), Leiden 2300, RC, The Netherlands

15 6) Gene Expression and Regulation Program, The Wistar Institute, Philadelphia, PA

16 7) Department of Clinical Genetics, Leiden University Medical Center, Leiden, The Netherlands

17 8) Corresponding author: Marco Trizzino, Department of Biochemistry and Molecular Biology, Sidney Kimmel  
18 Medical College, Thomas Jefferson University, 233 S 10<sup>th</sup> Street, BLSB 826, Philadelphia, PA, 19104. E-mail:  
19 [marco.trizzino@jefferson.edu](mailto:marco.trizzino@jefferson.edu)

20  
21 **Abstract**

22 The BAF complex modulates genome-wide chromatin accessibility. Specific BAF configurations have been  
23 shown to have functional consequences, and subunit switches are essential for cell differentiation.  
24 *ARID1B* and its paralog *ARID1A* encode for mutually exclusive BAF subunits. *De novo ARID1B*  
25 haploinsufficient mutations cause a neurodevelopmental disorder spectrum, including Coffin-Siris  
26 syndrome, which is characterized by neurological and craniofacial features. Here, we reprogrammed  
27 *ARID1B*<sup>+/-</sup> Coffin-Siris patient-derived skin fibroblasts into iPSCs, and investigated cranial neural crest cell  
28 (CNCC) differentiation. We discovered a novel BAF configuration (ARID1B-BAF), which includes ARID1B,  
29 SMARCA4, and eight additional subunits. This novel version of BAF acts as a gate-keeper which ensures  
30 exit from pluripotency and commitment towards neural crest differentiation, by attenuating pluripotency  
31 enhancers of the SOX2 network. At the iPSC stage, these enhancers are maintained in active state by an  
32 ARID1A-containing BAF. At the onset of differentiation, cells transition from ARID1A-BAF to ARID1B-BAF,  
33 eliciting attenuation of SOX2 enhancers and pluripotency exit. Coffin-Siris patient cells fail to perform the  
34 ARID1A/ARID1B switch, and maintain ARID1A-BAF at pluripotency enhancers throughout CNCC  
35 differentiation. This correlates with aberrant SOX2 binding at pluripotency enhancers, and failure to  
36 reposition SOX2 at developmental enhancers. SOX2 dysregulation promotes upregulation of the *NANOG*  
37 network, impairing CNCC differentiation. ARID1B-BAF directly modulates *NANOG* expression upon  
38 differentiation cues. Intriguingly, the cells with the most prominent molecular phenotype in multiple  
39 experimental assays are derived from a patient with a more severe clinical impairment.  
40 These findings suggest a direct connection between *ARID1B* mutations, CNCC differentiation, and a  
41 pathogenic mechanism for Coffin-Siris syndrome.

42  
43 **Keywords:** BAF, ARID1B, Coffin-Siris, pluripotency enhancers, NANOG, SOX2, neural crest, SALL4

44  
45  
46  
47  
48  
49

## 50 Introduction

51

52 Cell fate commitment is a complex process that requires timely regulation of developmental genes. This  
53 phenomenon is mediated by the concerted activity of transcription factors and chromatin regulators that  
54 modulate the interaction between *cis*-regulatory elements (enhancers, promoters) and RNA Polymerase  
55 II to elicit gene expression. In this framework, a key role is played by the Brg1/Brm associated factor (BAF)  
56 chromatin-remodeling complex. BAF leverages ATP to modulate nucleosome positioning and chromatin  
57 accessibility genome-wide<sup>1</sup>. Different configurations of BAF, with context specific functions, have been  
58 described, and switches between subunits have been reported to be linked to specific developmental  
59 stages<sup>2,3</sup>. All the known BAF configurations require the presence of a subunit containing an AT-rich DNA  
60 binding domain (ARID). Namely, in the BAF complex this function is carried out by two mutually exclusive  
61 subunits: ARID1A and ARID1B<sup>4-6</sup>. Previous studies in mouse embryonic stem cells (mESCs) have identified  
62 a mESC-specific configuration of BAF which regulates pluripotency and self-renewal of the embryonic  
63 stem cells (esBAF)<sup>4-6</sup>. Importantly, the esBAF exclusively incorporates ARID1A and not ARID1B. One of  
64 these studies also identified a non-canonical version of BAF (gBAF) not containing any ARID subunit and  
65 also involved in pluripotency maintenance of mouse embryonic stem cells<sup>4</sup>.

66 *De novo* haploinsufficient mutations in the *ARID1B* gene cause a spectrum of neurodevelopmental  
67 disorders, ranging from Coffin Siris syndrome to non-syndromic intellectual disability<sup>7-12</sup>. Coffin-Siris  
68 syndrome is associated with intellectual disability, specific craniofacial features, growth impairment,  
69 feeding difficulties and congenital anomalies such as heart and kidney defects<sup>13</sup>. Although other BAF  
70 components may also be mutated in this syndrome, the very large majority of mutations (~75%) are in  
71 *ARID1B*<sup>11,14,15</sup>. In addition to Coffin-Siris, genome-wide sequencing in unselected cohorts of patients with  
72 intellectual disability (ID) shows that *ARID1B* is always in the top-5 of causative genes, explaining about  
73 1% of all ID cases<sup>9,16</sup>. Studies in several mouse models were able to recapitulate the neurological  
74 phenotypes typical of the *ARID1B*-associated syndromes<sup>17-20</sup>. Nonetheless, the molecular function of  
75 ARID1B in cell fate commitment during human development is still poorly understood.

76 An important feature of *ARID1B* haploinsufficient individuals is represented not only by severe craniofacial  
77 abnormalities, but also by defects of the cardiac and digestive systems, often associated with ineffective  
78 migration of the cardiac and enteric neural crest<sup>12</sup>. Further, *ARID1B* is one of the most commonly mutated  
79 genes in neuroblastoma, a pediatric tumor of neural crest origin<sup>21</sup>. For all these reasons, the neural crest  
80 differentiation represents one of the most suitable models to study the consequences of *ARID1B*  
81 mutations in human development.

82 To investigate the molecular consequences of *ARID1B* haploinsufficient mutations in neural crest  
83 differentiation and craniofacial development, we reprogrammed skin fibroblasts of two unrelated  
84 *ARID1B*<sup>-/-</sup> Coffin-Siris patients into induced Pluripotent Stem Cells (iPSCs). Then we used these patient-  
85 derived iPSCs to specifically model Cranial Neural Crest Cell (CNCC) differentiation.

86 Thanks to this approach, we report the discovery of a novel BAF configuration, containing ARID1B,  
87 SMARCA4 and eight additional subunits (ARID1B-BAF). In line with the evidence that the esBAF and the  
88 gBAF do not contain ARID1B<sup>4-6</sup>, we demonstrate that *ARID1B* mutations do not affect self-renewal and  
89 pluripotency of human iPSCs. At this stage, the pluripotency is positively regulated by binding of an  
90 ARID1A-containing BAF to pluripotency-associated enhancers of the SOX2 and NANOG networks. On the  
91 other hand, we show that ARID1B-BAF plays an important role in lineage specification and exit from  
92 pluripotency. In fact, ARID1B-BAF is only transiently active during early stages of CNCC differentiation,  
93 where it replaces ARID1A-BAF at the SOX2/NANOG enhancers and elicits their repression. Intriguingly,  
94 ARID1B-BAF interacts with SALL4 (Spalt Like Transcription Factor 4), which is a multi-zinc-finger  
95 transcription factor essential for lineage commitment in early mammalian development, during which it  
96 targets sites with the same binding motifs also recognized by SOX2, OCT4 and NANOG<sup>22-25</sup>. This  
97 transcription factor can act as both activator and repressor and is dispensable for the maintenance of the

98 stem cell pluripotency networks, but it ensures that aberrant gene expression programs are not activated  
99 during lineage commitment<sup>23</sup>.

100 Importantly, we demonstrate that the *ARID1B*<sup>-/-</sup> Coffin-Siris cells are unable to switch from ARID1A-BAF  
101 to ARID1B-BAF at the onset of the CNCC differentiation, and instead maintain ARID1A-BAF at the  
102 pluripotency enhancers throughout the differentiation process. This leads to defective exit from  
103 pluripotency and impaired cranial neural crest differentiation. These findings provide evidence for a direct  
104 connection between *ARID1B* mutations and a pathogenic mechanism for ARID1B-associated  
105 neurodevelopmental syndromes.

106

107

## 108 **Results**

109

### 110 **Coffin-Siris patient-derived iPSCs are pluripotent and proliferate normally**

111 To investigate the function of ARID1B in craniofacial development, we obtained skin fibroblasts from two  
112 unrelated *ARID1B*<sup>-/-</sup> Coffin-Siris Syndrome patients (hereafter Patient-19 and Patient-26; Fig. 1a), one  
113 male and one female, both carrying previously identified *de novo* *ARID1B* mutations. In detail, Patient-19  
114 presented a nonsense mutation (c.3223C>T;p.Arg1075\*; Fig. 1b), while Patient-26 had a frameshift  
115 mutation (c.2598del;Tyr867Thrfs\*47; Fig. 1b)<sup>10,14</sup>. In both cases, a premature STOP codon was generated  
116 (Fig. 1b).

117 The fibroblasts were reprogrammed into iPSCs by the LUMC hiPSC Hotel (Leiden University). The patient-  
118 derived iPSCs exhibit regular morphology (Fig. 1c) and express the pluripotency genes, as shown by both  
119 immunofluorescence (Fig. 1d; Supplementary Fig. S1a,b) and RT-qPCR (Fig. 1e). Further, the patient-  
120 derived iPSCs grow at the same rate as an *ARID1B*<sup>+/+</sup> control line (Control line-1; Fig. 1f).

121 Importantly, the aberrant STOP codon introduced by the mutations is located either upstream (Patient-  
122 26) or inside (Patient-19) the AT-Rich Interactive Domain (ARID) (Fig. 1b), which is required for ARID1B's  
123 interaction with chromatin<sup>26</sup>. Moreover, in both patients, the new STOP codon is localized upstream of  
124 the Nuclear Localization Signal (NLS, Fig. 1b), suggesting that the gene product arising from the mutated  
125 allele would not be able to reach the nucleus and the chromatin even in the unlikely case that the  
126 transcript escaped non-sense mediated mRNA decay<sup>27</sup>. To test this, we performed cellular fractionation  
127 in patient and control iPSCs and conducted an ARID1B western blot on the chromatin fraction with an  
128 antibody raised against a peptide in the N-terminus of ARID1B, hence upstream of the mutated regions  
129 (sc-32762). Consistent with our hypothesis, the immunoblot on the chromatin fraction shows significantly  
130 lower ARID1B protein level in the two patients relative to an *ARID1B*<sup>+/+</sup> iPSC line (Control line-1;  
131 Supplementary Figure S1c). No ARID1B signal was detected in any of the lines in the cytoplasmic fraction  
132 (Supplementary Fig S1c).

133 In summary, *ARID1B* haploinsufficient iPSCs are pluripotent, do not exhibit growth defects, but display  
134 significantly less chromatin-bound ARID1B.

135

### 136 **The CNCC differentiation is impaired in Coffin-Siris patient-derived iPSCs**

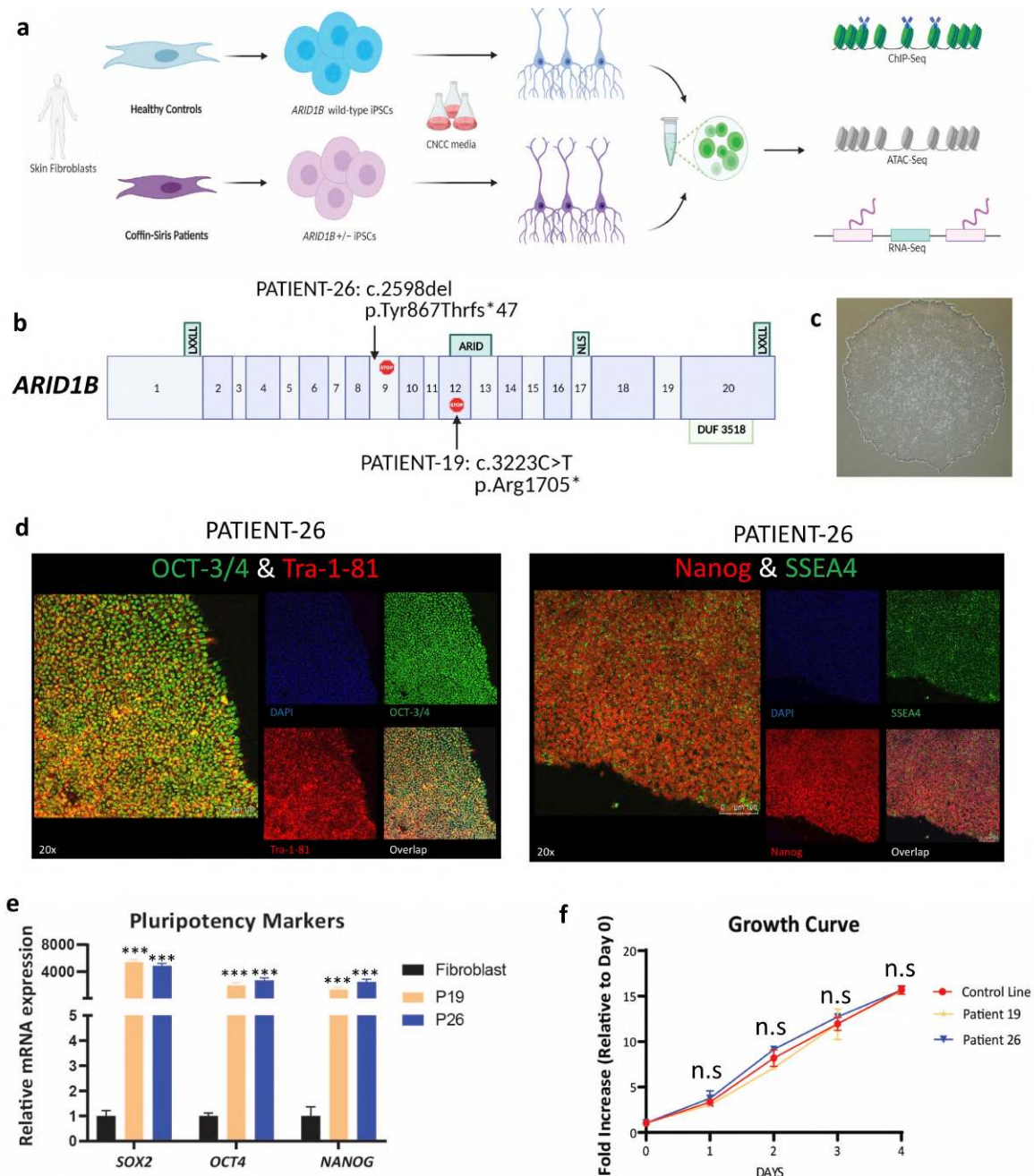
137 We took advantage of a published CNCC differentiation protocol<sup>28</sup>, and using Control line-1 we obtained  
138 fully differentiated Cranial Neural Crest Cells in 14 days (Fig. 2a,b). A time-course western blot conducted  
139 during the CNCC differentiation of Control line-1 revealed that ARID1B protein is highly expressed only  
140 during the first week of differentiation, peaking between days 5 and 7, after which is markedly  
141 downregulated (Fig. 2c).

142

143

144

145



146 **Figure 1 – iPSCs derived from Coffin-Siris patients are pluripotent and proliferate normally.** (a) Study  
 147 system: iPSCs were derived from skin fibroblasts of two unrelated Coffin-Siris patients. The iPSCs were  
 148 used in this study to generate Cranial Neural Crest Cells (CNCCs) and perform genomic experiments to  
 149 investigate the effect of *ARID1B* mutations. (b) Graphical illustration of the *ARID1B* haploinsufficient  
 150 mutations affecting the two studied patients. The numbers in the gene model refer to *ARID1B*'s isoform  
 151 NM\_020732.3. (c) Colony of iPSCs derived from Patient-19 showing typical iPSC morphology. (d, e)  
 152 Immunofluorescence and rt-qPCR quantifying the expression of the key pluripotency markers in iPSCs  
 153 derived from Patient-26. (f) Growth curve comparing an *ARID1B*-wt Control iPSC Line with the two patient  
 154 lines. The patient cells do not exhibit growth impairment.

155  
 156



157 Next, we induced the differentiation in the two Coffin-Siris lines and the Control line-1 together, and used  
 158 flow cytometry to measure multiple pluripotency (SSEA-4, TRA-1-60-R) and CNCC (CD10, CD99) surface  
 159 markers. The cells were sampled at day-zero (iPSC stage), day-5 (mid-point), and day-14 (end of  
 160 differentiation). Notably, the differentiation was impaired in both patient lines. In fact, in both lines we  
 161 identified a sizable cell population still double-positive for the pluripotency surface markers even after 14  
 162 days (Fig. 2d). This pluripotent population comprised 4.36% and 19.5% of the cells in the two patient  
 163 lines, respectively (Fig. 2d). In line with this, relative to the control line, a large fraction of the patient cells  
 164 showed significantly lower expression of the CNCC surface markers even after 14 days of differentiation  
 165 relative to the control line (Fig. 2e). Together, our data suggest that while *ARID1B* is dispensable for  
 166 pluripotency, haploinsufficiency of this gene is enough to severely impair differentiation into CNCCs.

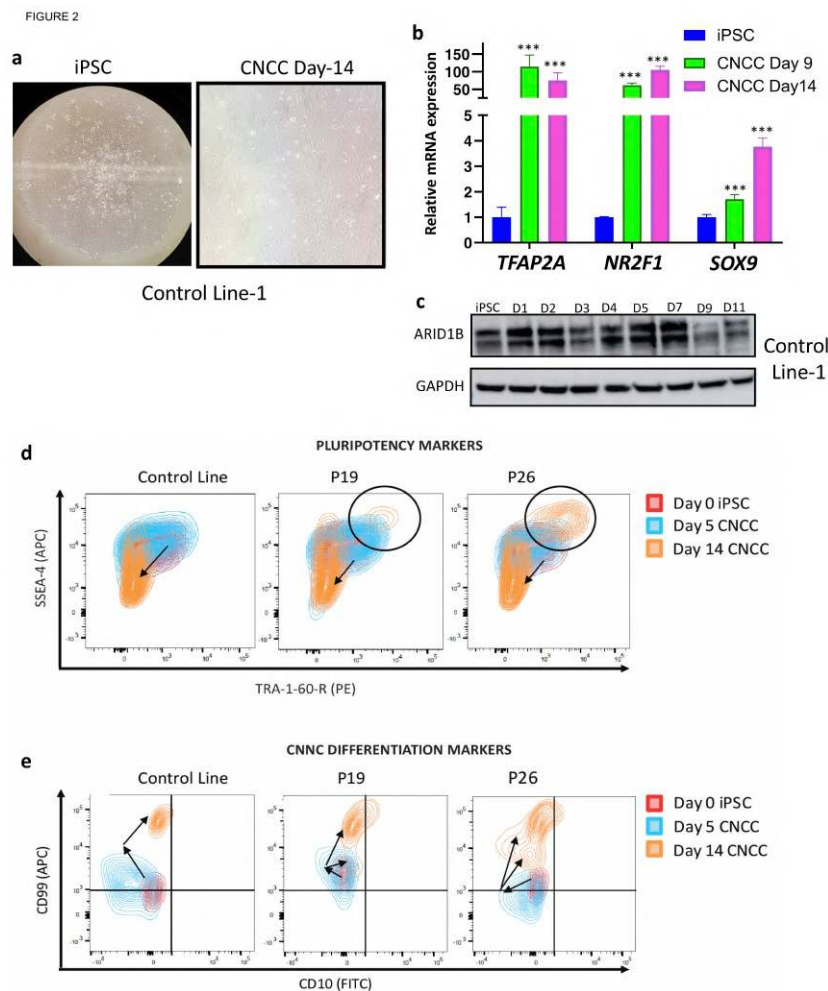


**Figure 2 – CNCC differentiation is impaired in the patient cells. (a, b)** CNCC differentiation was optimized using an *ARID1B*-wt Control Line. After 14 days, the cells exhibited the classic CNCC morphology and expressed the CNCC markers. **(c)** Time-course immunoblot conducted using Control Line-1 during CNCC differentiation shows that *ARID1B* is active in the first 7 days of the differentiation, with a peak of activity between day-5 and day-7. The *ARID1B* protein level strongly decreases after day-7. **(d, e)** Flowcytometry quantifying expression of surface markers for pluripotency and CNCC differentiation in control line-1 and in the two patient lines. A large cell population is still pluripotent in both patients after 14 days (d). The patient lines also show reduced expression of CNCC surface markers after 14 days of differentiation relative to an *ARID1B*-wt Control Line at the same time point (e).

## 205 **Chromatin accessibility is dysregulated in the differentiating patient cells**

206 We used Next-Generation Sequencing to investigate why *ARID1B* haploinsufficient Coffin-Siris iPSCs did  
207 not successfully differentiate into CNCCs. Given that ARID1B protein levels in control cells reach a peak  
208 between days 5 and 7, we selected day-5 as a time-point to collect the genomic data. The experiments  
209 were conducted with two biological replicates per condition (two control lines, two patient lines). For  
210 each condition, a male and a female were included to avoid sex-specific confounding effects. Technical  
211 replicates were also performed for each biological replicate. To avoid batch effects, all the biological  
212 replicates and conditions were processed together.

213 Since ARID1B is a component of the BAF chromatin-remodeling complex, we profiled chromatin  
214 accessibility with ATAC-seq. Overall, we detected 29,758 ATAC-seq peaks replicated across all replicates  
215 and all conditions (patients and controls; FDR <0.05; Fig. 3a). Conversely, 5,540 peaks were specific to the  
216 patients (i.e. replicated in all the patient replicates and not detected in any of the controls; hereafter  
217 patient-specific ATAC-seq regions; Fig. 3a,b; Supplementary File S1). Finally, only 578 peaks were specific  
218 to the controls (hereafter control-specific ATAC-seq regions; Fig. 3a,c; Supplementary File S1).

219 We therefore focused on the 5,540 patient-specific ATAC-seq regions because they represented 91%  
220 (5,540/6,118) of all regions with differential chromatin accessibility between patients and controls.  
221 ARID1B ChIP-seq performed in the Control Line-1 at the day-5 shows ARID1B binding in all of these regions  
222 (Fig. 3d). This suggests that the chromatin accessibility in the 5,540 patient-specific ATAC-seq regions may  
223 be directly regulated by ARID1B-BAF. In line with this, ARID1B ChIP-seq performed on all four lines at day-  
224 5 of differentiation confirmed that the 5,540 patient-specific ATAC-seq regions are similarly bound by  
225 ARID1B in both control lines, while the binding is almost entirely lost in both patient lines (Supplementary  
226 Fig. S2a).

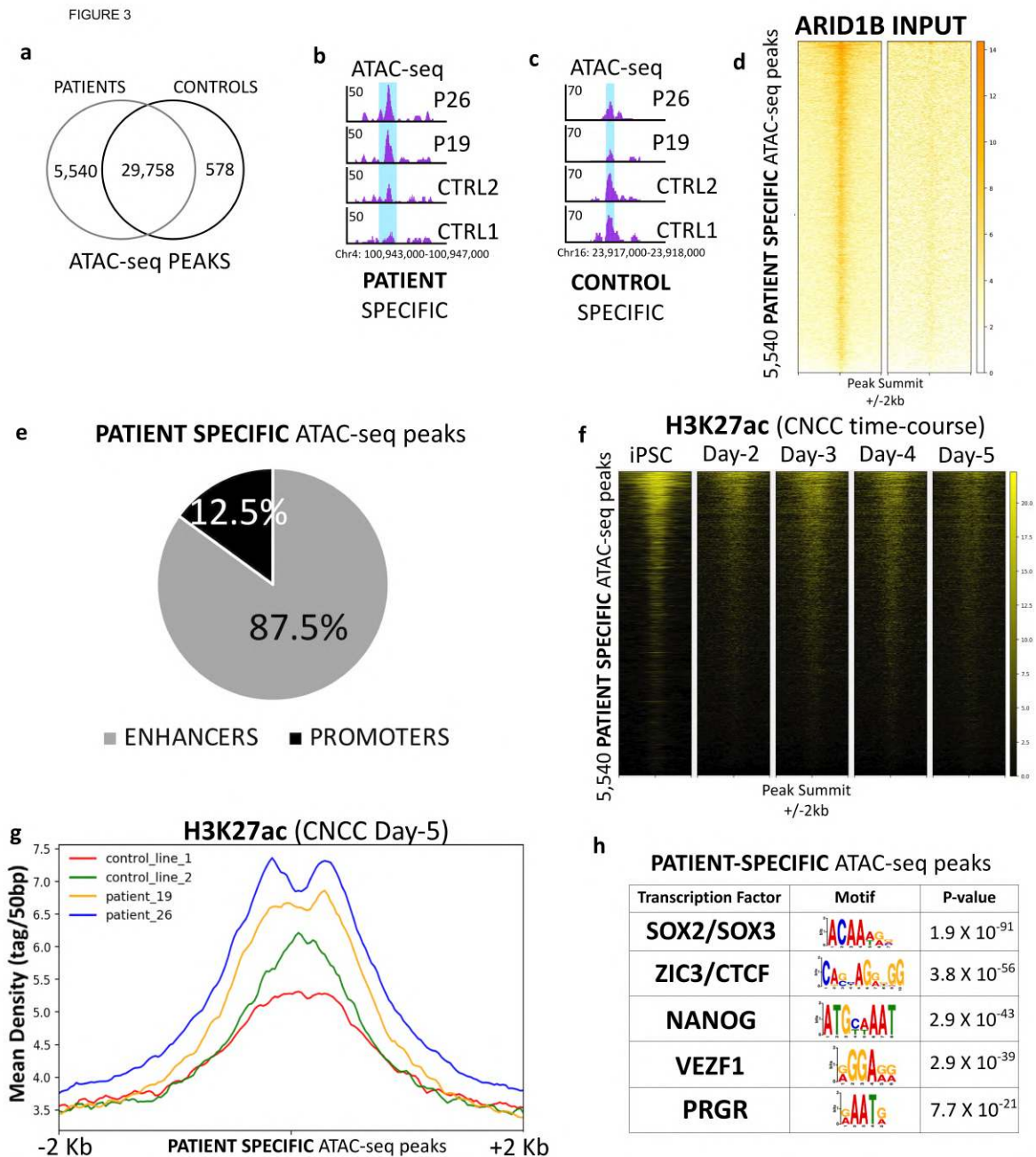
227

## 228 **The ARID1B-BAF attenuates thousands of enhancers at the onset of CNCC differentiation**

229 To determine the genomic nature of these regions, we associated a gene to each region based on the  
230 distance from the nearest Transcription Start Site (TSS). Overall, 87.5% of the ARID1B ChIP-seq peaks  
231 were located >10 Kb from the nearest TSS and may represent putative enhancers, while the remaining  
232 12.5% are likely promoters (Fig. 3e). ChIP-seq time-course for H3K27ac in Control Line-1 revealed that  
233 many of these regulatory regions are enriched for H3K27ac in iPSCs, while their regulatory activity  
234 progressively decreases upon differentiation cues, and by day-5 very little H3K27ac signal is detectable  
235 (Fig. 3f). Notably, the gradual decrease in H3K27ac mirrors the steady increase in ARID1B expression  
236 detected during the early stages of CNCC differentiation (Fig. 2c). Consistently, the differentiating CNCCs  
237 of both patients have significantly higher levels of H3K27ac in these regions relative to the two control  
238 lines at the day-5 (Wilcoxon's Rank Sum Test  $p < 2.2 \times 10^{-16}$  in all the patient vs control pairwise  
239 comparisons; Fig. 3g).

240 Based on the high H3K27ac signal that the 5,540 patient-specific regions display at the iPSC stage (Fig. 3f),  
241 we surmised that these sites could represent cis-regulatory elements important for pluripotency. In line  
242 with this hypothesis, DNA-motif analysis on the 5,540 regions revealed that they are enriched for the  
243 binding sites of multiple pluripotency factors, including SOX2 and NANOG (Fig. 3h; Supplementary File S2).  
244 Next, we wanted to ensure that the molecular phenotypes observed so far were directly caused by the  
245 *ARID1B* mutations, and not by co-occurring mutations in other genes coincidentally shared by both  
246 (unrelated) patients. Hence, we employed shRNAs to knock-down ARID1B in the Control Line-1. We were  
247 able to obtain a partial knock-down of ARID1B at the iPSC stage (shRNA-1; Supplementary Fig. 2b), which  
248 represented a suitable model for *ARID1B* haploinsufficiency. We differentiated the ARID1B-KD iPSCs  
249 towards CNCC and again collected the cells at the day-5, and performed ATAC-seq and ChIP-seq for  
250 H3K27ac. Notably, both sequencing experiments perfectly recapitulated what we previously observed in  
251 the patient lines.

252



253 **Figure 3 – Chromatin remodeling at pluripotency enhancers is dysregulated in the patient cells.** (a) At  
 254 CNCC day-5, 29,758 ATAC-seq peaks are shared between patient and control lines. 5,540 peaks are specific  
 255 of the patients. 578 peaks are specific of the control lines. (b) UCSC Genome Browser example of a  
 256 PATIENT-SPECIFIC ATAC-seq peak. (c) UCSC Genome Browser example of a CONTROL-SPECIFIC ATAC-seq  
 257 peak. (d) ARID1B ChIP-seq heatmaps (Control Line-1; CNCC Day-5) show ARID1B binding at nearly all of  
 258 the PATIENT-SPECIFIC ATAC-seq peaks. The input (collected at CNCC Day-5) was used as a control (e)  
 259 87.5% of the PATIENT-SPECIFIC ATAC-seq peaks are located > 1kb from a TSS. (f) Heatmaps of H3K27ac  
 260 ChIP-seq time-course at the 5,540 PATIENT-SPECIFIC ATAC-seq peaks (Control Line-1). (g) H3K27ac ChIP-  
 261 seq average profiles centered on the PATIENT-SPECIFIC ATAC-seq regions (CNCC Day-5). (h) Motif analysis  
 262 at the PATIENT-SPECIFIC ATAC-seq regions revealed enrichment for the binding motif of multiple  
 263 pluripotency factors.



264 Namely, upon ARID1B-KD, we detected significantly increased chromatin accessibility and H3K27ac signal  
265 in the 5,540 patients-specific regions relative to the same iPSC line transduced with a control shRNA  
266 (Wilcoxon's Rank Sum Test  $p < 2.2 \times 10^{-16}$ ; Supplementary Fig. S2c,d).  
267 Together, these data indicate that ARID1B-BAF modulates the chromatin accessibility of a specific set of  
268 ~4,900 pluripotency enhancers and ~600 promoters that are highly active at the iPSC stage, moderately  
269 active at the CNCC differentiation onset, and inactive by day-5 (Fig. 3f). We find that the attenuation of  
270 these cis-regulatory elements is impaired in the *ARID1B* haploinsufficient cells, which likely hampers the  
271 entire differentiation process towards CNCCs.

272  
273

#### 274 **"Pluripotency" and "Exit from Pluripotency" genes are dysregulated in the differentiating patient cells**

275 Impaired attenuation of ~4,900 pluripotency-relevant enhancers and ~600 promoters could have a  
276 profound effect on gene expression levels. Indeed, RNA-seq conducted on the four lines at CNCC Day-5  
277 identified 2,356 differentially expressed genes, 1,685 of which were downregulated, and 671 upregulated  
278 (FDR <5%; Fig. 4a). As expected, *ARID1B* was one of the top downregulated genes in patient CNCCs at the  
279 day-5 (Fig. 4a). In stark contrast, only 54 genes were identified as differentially expressed when we  
280 performed RNA-seq at the iPSC stage (FDR <5%). This suggests that ARID1B has an important function  
281 upon lineage commitment, again mirroring the progressive increase in the ARID1B protein level observed  
282 during early differentiation (Fig. 2c). These findings are consistent with previous studies that  
283 demonstrated that the mESC BAF complexes (esBAF, gBAF) do not include ARID1B<sup>4-6</sup>.  
284 Notably, 598/2,356 (25.4%) of the genes differentially expressed at CNCC day-5 also represented the  
285 nearest gene to one of the 5,540 pluripotency enhancers and promoters aberrantly active in the Coffin-  
286 Siris patient cells at the same time point (Fisher's Exact Test  $p < 0.0001$ ; Supplementary File S3). These  
287 results suggest that over a quarter of the differentially expressed genes are under the direct control of  
288 ARID1B-BAF throughout modulation of the chromatin accessibility at the associated enhancers and  
289 promoters. As expected, when we compared these 598 genes against the entire set of differentially  
290 expressed genes, we found that the 598 genes exhibit enrichment for genes upregulated in patients  
291 (Fisher's Exact Test  $p < 0.0001$ ), likely determined by increased activity in the associated enhancers and  
292 promoters.

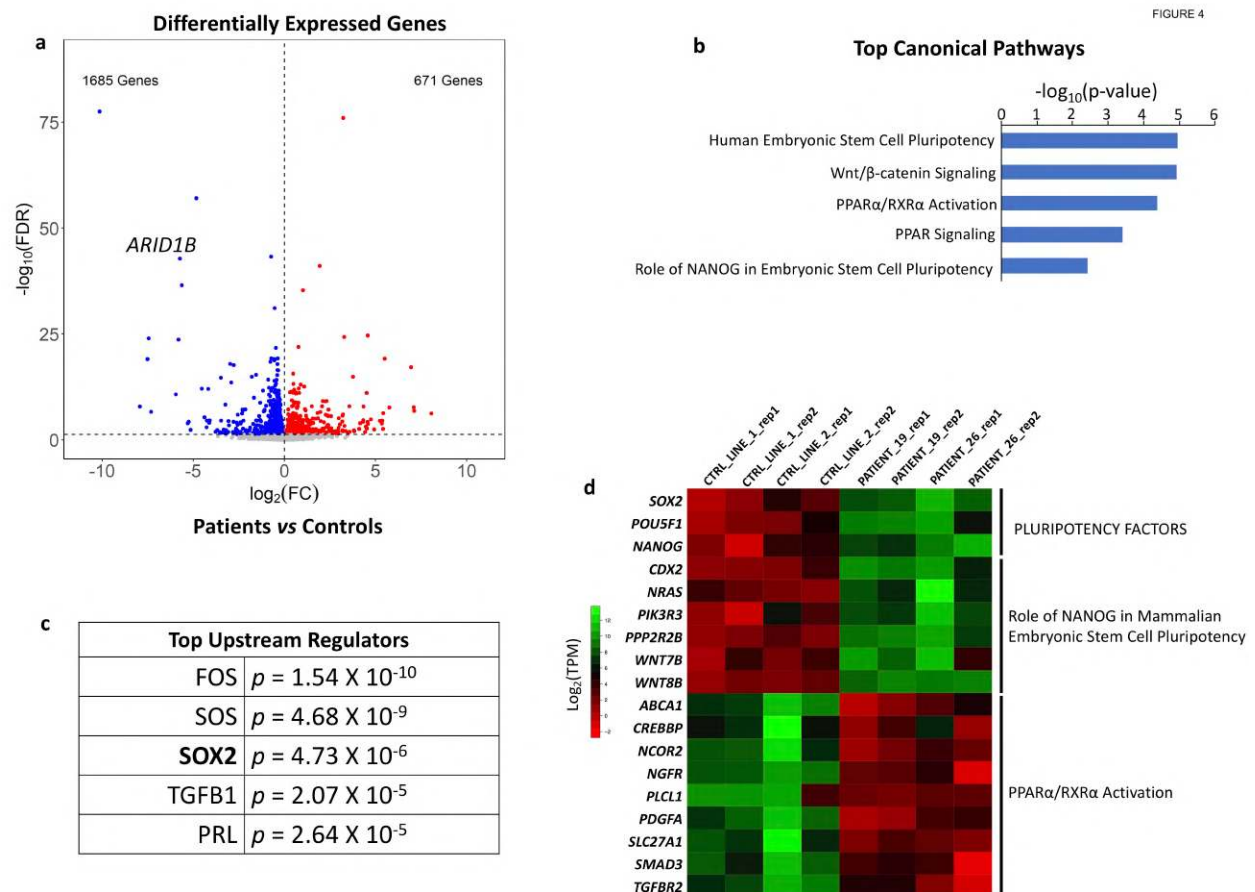
293 Ingenuity Pathway Analysis on the 598 genes identified five of the top canonical pathways as associated  
294 with either pluripotency or exit from pluripotency (Fig. 4b; Supplementary File S4). Wnt- $\beta$  catenin  
295 signaling pathway was also found as enriched. An association between ARID1B and this specific pathway  
296 was suggested in recent studies<sup>29,30</sup>.

297 In accordance with the ATAC-seq data, SOX2 was detected among the top upstream regulators (Fig. 4c),  
298 and three of the most important pluripotency factors, and specifically *NANOG*, *SOX2* and *POU5F1* (OCT4),  
299 were found as still highly expressed in the patient lines at the day-5 (Fig. 4d).

300 Both the "*Role in NANOG in Mammalian Embryonic Stem Cell Pluripotency*" pathway and the  
301 "*PPAR $\alpha$ /RXR $\alpha$  Activation*" pathway were enriched in the 598 genes (Fig. 4b). Namely, the genes belonging  
302 to the former pathway were all upregulated, while the genes belonging to the latter were downregulated  
303 (Fig. 4d). These two pathways caught our attention because they are thought to antagonize each other.  
304 More specifically, NANOG blocks the differentiation of pluripotent cells and establishes the pluripotent  
305 state during somatic cell reprogramming. On the other hand, the PPAR $\alpha$ /RXR $\alpha$  pathway is activated at  
306 the onset of differentiation to promote exit from pluripotency<sup>31</sup>. The activation of PPAR $\alpha$ /RXR $\alpha$  elicits the  
307 repression of the *NANOG* network to allow efficient exit from the undifferentiated stage<sup>31-33</sup>. Consistent  
308 with this, PPAR $\alpha$ -inhibitors have been employed to enhance and improve iPSC reprogramming<sup>31</sup>.

309 Taken together, our RNA-seq data suggest that the differentiating *ARID1B*<sup>+/-</sup> patient lines exhibit a  
310 persistent upregulation of multiple pluripotency factors and associated gene networks, along with

311 downregulation of genes responsible for exit from pluripotency, which impairs the differentiation  
 312 program to CNCC.  
 313

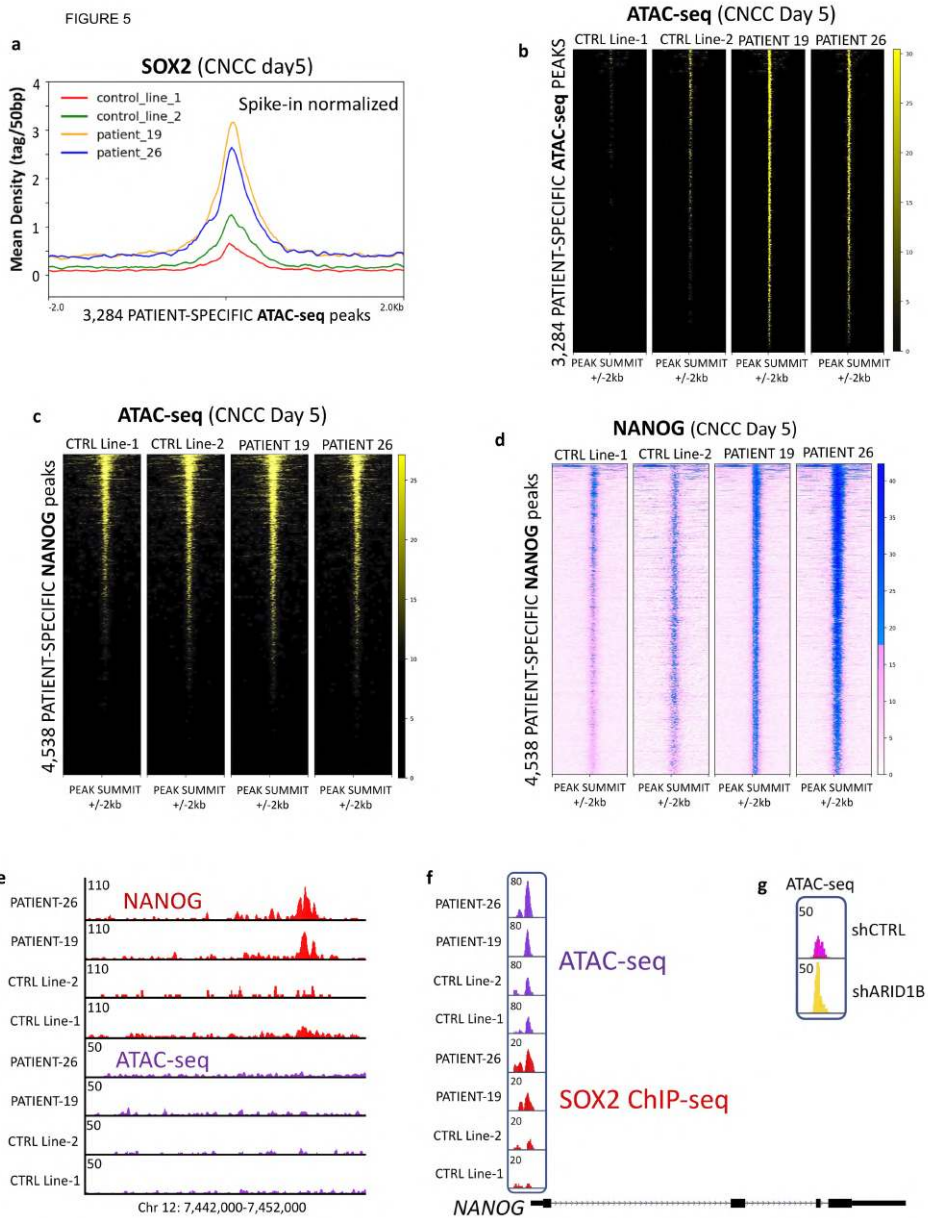


314  
 315  
 316 **Figure 4 – “Pluripotency” and “Exit from Pluripotency” genes are dysregulated in differentiating patient**  
 317 **CNCCs. (a)** RNA-seq volcano plot shows the differentially expressed genes between patient and control  
 318 lines at CNCC Day-5. *ARID1B* is one of the top downregulated genes. **(b)** Top canonical pathways (IPA  
 319 analysis) enriched in the set of 598 differentially expressed genes that also represent the closest gene to  
 320 a PATIENT-SPECIFIC ATAC-seq peak. **(c)** Top upstream regulators (IPA analysis) enriched in the same set  
 321 of 598 genes used for panel b. **(d)** RNA-seq heatmap displaying expression patterns at CNCC Day-5 for  
 322 pluripotency genes, for genes of the NANOG network, and for genes associated to exit from pluripotency  
 323 (PPAR $\alpha$ /RXR $\alpha$  activation pathway).

324  
 325  
 326 **Aberrant SOX2 and NANOG activity in the *ARID1B* haploinsufficient patient cells**  
 327 Our experiments indicate that the *ARID1B* haploinsufficient cells fail to attenuate thousands of  
 328 pluripotency enhancers and promoters enriched for SOX2 and NANOG binding sites (Fig. 3a–h). Further,  
 329 at day-5 of CNCC differentiation, the expression of SOX2 and NANOG is significantly higher in the patient  
 330 derived cells than in the controls, and the gene regulatory networks associated with these pluripotency  
 331 factors are also upregulated (Fig. 4b–d).

332 Given these results, we set out to investigate the binding profile of SOX2 and NANOG in patient and  
333 control lines by ChIP-seq at CNCC day-5. Our spike-in normalized SOX2 ChIP-seq revealed that 3,284/5,540  
334 (59.7%) patient-specific ATAC-seq peaks are characterized by significantly higher SOX2 binding in patients  
335 relative to the control lines. In line with this, the chromatin at these regions is accessible in the patient  
336 lines but not in the control lines (Fig. 5b). SOX2 is a pioneer factor that is able to bind condensed  
337 nucleosomes to open the chromatin for the binding of other factors<sup>34</sup>. As demonstrated by previous  
338 studies in mouse in embryonic stem cells SOX2 and other pluripotency pioneer factors (e.g. OCT4) require  
339 the BAF complex to perform their pioneer activity<sup>6,34,35</sup>. Our findings indicate that in control conditions  
340 ARID1B-BAF complex likely antagonizes the cooperation between other BAF configurations and SOX2,  
341 counter-acting the pioneer activity of the latter as soon as the cell differentiation is induced. Further, we  
342 identified an additional set of 497 SOX2 peaks specific of the patient lines, which did not exhibit changes  
343 in chromatin accessibility. Moreover, we also identified 1,146 SOX2 peaks exclusive of the control lines  
344 (Supplementary File S5). Importantly, these control-specific SOX2 peaks were located in proximity to  
345 genes associated with neural crest differentiation, including *TFAP2A*, *PAX6*, *PAX7*, *WNT4*, *ENO1*, *C8B*, and  
346 *SERBP1* among others. These findings are consistent with two recent studies which suggested that SOX2-  
347 chromatin interactions are rewired upon differentiation cues<sup>36,37</sup>. Such rewiring appears impaired in  
348 *ARID1B*-haploinsufficient cells, which aberrantly maintain SOX2 at the pluripotency-associated enhancers,  
349 and at the same time fail to reposition this transcription factor at the developmental enhancers.  
350 Next, we profiled NANOG at day-5 of differentiation. For this transcription factor, the spike-in normalized  
351 ChIP-seq revealed 4,538 peaks unique to the patients (Supplementary File S6). However, in this case, only  
352 219 (4.8%) of the patient-specific NANOG peaks overlapped a patient-specific ATAC-seq peak. We thus  
353 interrogated our ATAC-seq data to determine the state of chromatin accessibility at the 4,538 patient-  
354 specific NANOG peaks, and overall found no significant changes in accessibility in these regions between  
355 the patients and the control lines (Fig. 5c). Notably, nearly a quarter of the patient-specific NANOG peaks  
356 were found in regions of repressed chromatin (Fig. 5c,e), consistent with recent studies which suggested  
357 that NANOG can bind repressed chromatin like other pioneer pluripotency factors<sup>38,39</sup>.  
358 Despite no changes in chromatin accessibility, the NANOG ChIP-seq signal at the 4,538 patient-specific  
359 NANOG peaks was significantly higher in the patient than in the control lines (Wilcoxon's Rank Sum Test  
360  $p < 2.2 \times 10^{-16}$  in all the patient vs control pairwise comparisons; Fig. 5d,e). We hypothesized that the  
361 increased NANOG binding detected in the patients' cells (Fig. 5d) could reflect increased *NANOG*  
362 expression (Fig. 4d). In fact, several elegant studies in embryonic stem cells have demonstrated that the  
363 downregulation of *NANOG* gene expression marks the transition from naïve to primed state<sup>40-42</sup>.  
364 Importantly, it has been shown that *NANOG* expression is modulated by SOX2, which binds a cis-  
365 regulatory element in the promoter region of *NANOG*<sup>43,44</sup>. Thus, we examined this cis-regulatory element  
366 in detail. As expected, at day-5 of CNCC differentiation, the chromatin accessibility at the promoter-  
367 proximal element is significantly higher in the two patient lines than in the two controls (Student's T-Test  
368  $p=0.0065$ ; Fig. 5f). Accordingly, increased chromatin accessibility correlates with increased SOX2 binding  
369 on the cis-regulatory element (Fig. 5f), perhaps explaining the higher *NANOG* gene expression reported in  
370 patients at CNCC day-5. Lastly, our shRNA experiments also replicated these findings, demonstrating that  
371 the knock-down of ARID1B in the Control line-1 line correlates with a sizeable increase in accessibility at  
372 the *NANOG* cis-regulatory element (Fig. 5g), thus suggesting that ARID1B-BAF directly modulates *NANOG*  
373 expression dosage at the onset of differentiation.  
374 In sum, the *ARID1B* haploinsufficient lines exhibit persistent activity of two key pluripotency factors (SOX2,  
375 NANOG) in the early stages of CNCC differentiation. The aberrant activity of SOX2 and NANOG leads to  
376 impaired lineage commitment and inefficient CNCC differentiation.

377  
378  
379



380  
381  
382  
383  
384  
385  
386  
387  
388  
389  
390  
391  
392  
393

**Figure 5 – Aberrant SOX2 and NANOG activity in the patient cells at CNCC Day-5.** (a) SOX2 ChIP-seq average profile for 3,284 patient-specific ATAC-seq peaks showing patient-specific SOX2 signal (spike-in normalized; CNCC Day-5). (b) ATAC-seq heatmaps at the 3,284 peaks shown in Fig. 5a reveal that these regions display increased chromatin accessibility in the patients relative to the two control lines. (c) ATAC-seq heatmaps at 4,538 patient-specific NANOG peaks display no changes in accessibility between patient and control lines. (d) NANOG ChIP-seq heatmaps at 4,538 patient-specific NANOG peaks (spike-in normalized; CNCC Day-5). (e) Example of patient-specific NANOG peak in a region with no chromatin accessibility (CNCC Day-5). (f) At CNCC Day-5, a cis-regulatory element in the promoter region of *NANOG* is more accessible in the patients than in the control lines. The same element also displays higher SOX2 binding in the patients than in the controls. (g) Knock-down of ARID1B from Control Line-1 also elicits an increase in chromatin accessibility at the cis-regulatory element in the promoter region of *NANOG* (CNCC Day-5).



### 394 **A switch from ARID1A-BAF to ARID1B-BAF is necessary for exit from pluripotency**

395 We wanted to elucidate how the BAF complex compensates for *ARID1B* haploinsufficiency. As mentioned  
396 earlier, ARID1A and ARID1B represent the only two subunits of the BAF harboring an ARID domain, which  
397 is leveraged by the complex to interact with the chromatin<sup>26</sup>. A third ARID subunit (ARID2) is exclusive of  
398 a different configuration of the complex (pBAF). *ARID2* mutations have shown to cause a  
399 neurodevelopmental disorder that does not fully fit the Coffin-Siris syndrome phenotype, although there  
400 is some overlap<sup>45</sup>. Compensation mechanisms between ARID1A and ARID1B were recently demonstrated  
401 in ovarian cancer<sup>46</sup>. We hence hypothesized that the *ARID1B* haploinsufficient patient cells may  
402 compensate for partial loss of ARID1B with ARID1A. To test this, we first assessed ARID1A protein levels  
403 in *ARID1B*-wt cells during the course of CNCC differentiation and found that ARID1A exhibits a pattern of  
404 activity complementary to ARID1B (Fig. 6a). In agreement with the specific composition of the esBAF,  
405 which requires ARID1A<sup>5,6</sup>, the human iPSCs show high ARID1A protein level and relatively low ARID1B (Fig.  
406 6a). On the other hand, on day-1 of CNCC differentiation ARID1B is immediately upregulated while the  
407 ARID1A protein is completely repressed and is no longer detectable (Fig. 6a). ARID1B remains the only  
408 active ARID1 subunit between day-1 and day-7 (Fig. 6a). Finally, after day-7, ARID1B is abruptly  
409 downregulated while high ARID1A protein level is reprinted (Fig. 6a). Together, these data suggest  
410 that in *ARID1B*-wt conditions the differentiating CNCCs perform multiple switches between ARID1A and  
411 ARID1B, the most critical likely taking place as soon as the differentiation is induced. We previously  
412 identified the time-frame between days 5 and 7 as the peak of ARID1B expression during CNCC  
413 differentiation (Figs. 2c and 6a). In this time-frame ARID1A is not active in wild-type conditions (Fig. 6a).  
414 Nonetheless, the differentiating cells from both patients present high ARID1A protein levels at this time  
415 point, as opposed to almost no detectable protein in the Control line (Fig. 6b). This confirms that patient  
416 cells compensate for the partial loss of ARID1B by maintaining high ARID1A levels throughout the  
417 differentiation process. A recent study conducted on liver cells demonstrated that ARID1A-containing  
418 BAF and ARID1B-containing BAF may have antagonistic function in the transcriptional regulation of  
419 specific genes, with ARID1B acting prevalently as a repressor of enhancer elements, as opposed to the  
420 ARID1A, which mostly behaves as an activator<sup>47</sup>. Hence, we hypothesized that the aberrantly high ARID1A  
421 protein levels detected in the patient-derived cells during CNCC differentiation might underlie the long-  
422 lasting activity of the pluripotency enhancers. Consistently, ARID1A-ChIP followed by qPCR revealed that  
423 the pluripotency enhancers are bound by ARID1A at the iPSC stage in both the control and the patient  
424 lines at comparable levels (Fig. 6c; *p-values* in Supplementary File S7). On the other hand, at the day-5  
425 ARID1A binding is completely lost in the control lines – which have meanwhile gained ARID1B at the same  
426 sites (Fig. 3d) – while it is maintained in both patient lines (Fig. 6c; *p-values* in Supplementary File S7).  
427 To confirm genome-wide that all the 5,540 pluripotency enhancers are bound by ARID1A in the patients,  
428 we performed ARID1A ChIP-seq in the patient lines at day-5 of CNCC differentiation. In agreement with  
429 the ChIP-qPCR data, the ChIP-seq demonstrated that all the 5,540 pluripotency elements are bound by  
430 ARID1A in both patients at CNCC Day-5 (Fig. 6d). The persistent binding of the ARID1A-BAF at the  
431 pluripotency enhancers could perhaps explain why the patient cells do not efficiently repress these  
432 regions at the onset of the neural crest differentiation.

### 433 434 **The ARID1B-BAF complex exclusively incorporates SMARCA4 as ATPase subunit**

435 Finally, we designed a set of experiments to shed light on the composition of the ARID1B-BAF at the day-  
436 5 of CNCC differentiation. Thus, we performed immunoprecipitation of endogenous ARID1B followed by  
437 mass-spectrometry (IP-MS) in Control Line-1. With this approach, ARID1B coeluted with a total of 9  
438 additional BAF subunits (Fig. 6d). In mammals, the BAF complexes can incorporate two widely  
439 interchangeable and mutually exclusive ATPase subunits (i.e. SMARCA2, and SMARCA4). Remarkably,  
440 SMARCA4 was the only ATPase subunit identified as coeluting with ARID1B in our IP-MS, while zero  
441 peptides of SMARCA2 were detected (Fig. 6e).

442  
443  
444  
445  
446  
447  
448  
449  
450  
451  
452  
453  
454  
455  
456  
457  
458  
459  
460  
461  
462  
463  
464  
465  
466  
467  
468  
469  
470  
471  
472  
473  
474  
475  
476  
477  
478  
479  
480  
481  
482  
483  
484  
485  
486  
487  
488  
489

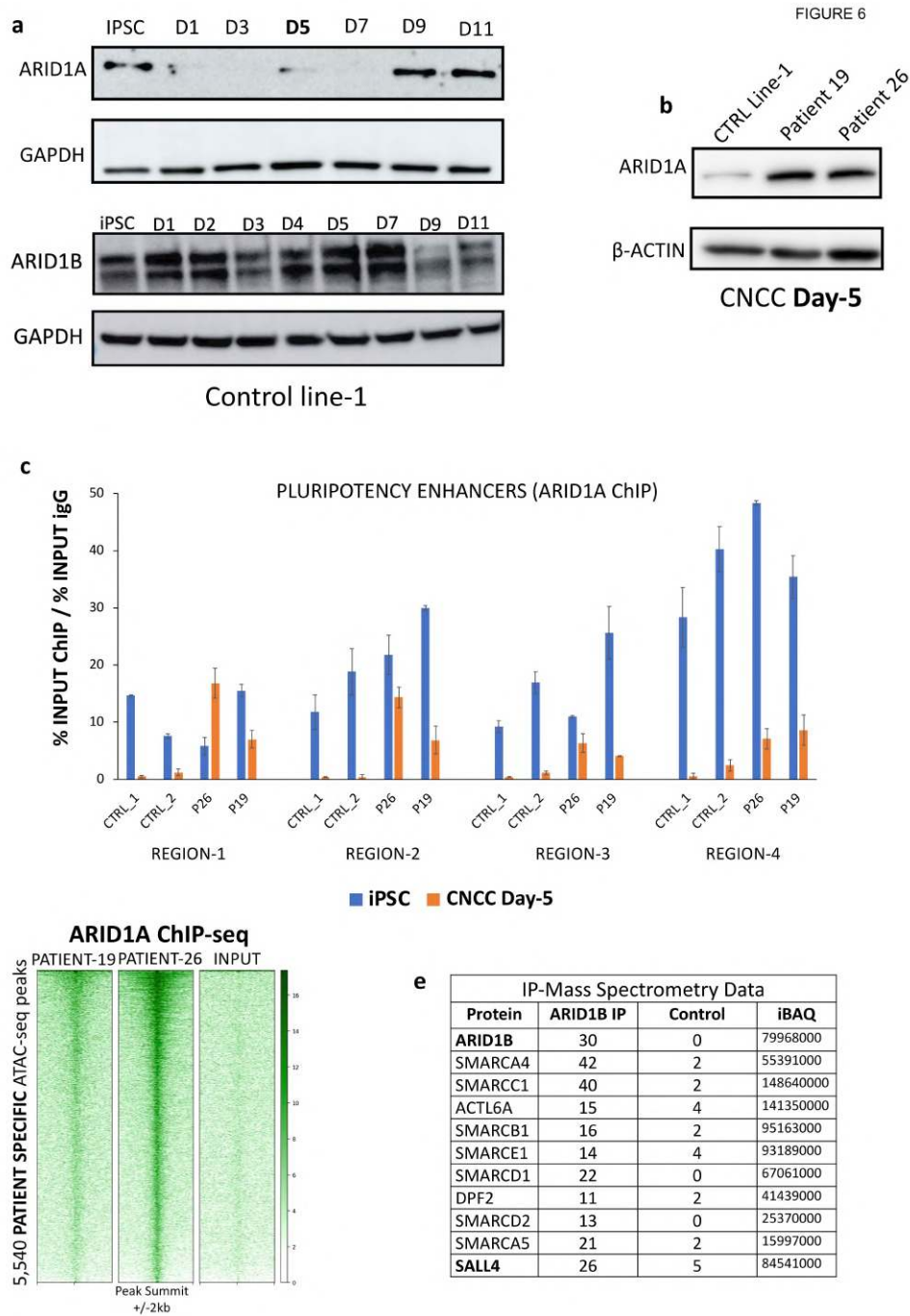


**Figure 6 – A switch between ARID1A-BAF and ARID1B-BAF is required for a successful exit from pluripotency. (a)** Time-course immunoblot conducted using Control Line-1 during CNCC differentiation shows that ARID1A is active at the iPSC stage, and abruptly downregulated at day-1 of differentiation. ARID1A protein level is upregulated again after day-7, mirroring ARID1B’s downregulation at the same time point (ARID1B blot duplicated here from Fig. 2c for convenience). **(b)** ARID1A immunoblot: both patient lines display aberrantly high ARID1A’s protein level at CNCC Day-5. **(c)** ChIP-qPCR of ARID1A at select pluripotency enhancers: at the iPSC stage the enhancers are bound by ARID1A comparably in both patient and control lines. At CNCC Day-5, the binding is completely lost in the patients while it is at least partially maintained in the patient lines. Coordinates and p-values (T-Test) in Supplementary File S7. **(d)**

490 ChIP-seq for ARID1A in the two patient lines at CNCC Day-5. Heatmaps are centered on the 5,540  
491 pluripotency enhancers. Input collected at CNCC Day-5 was used as a control. (e) Table displaying all the  
492 BAF subunits (plus SALL4) that coeluted with ARID1B in the IP-MS performed at Day-5 of CNCC5  
493 differentiation in Control Line-1. Values represent unique peptide numbers. iBAQ values are shown in  
494 last column.

495  
496  
497 This suggests that ARID1B-BAF selectively incorporates only SMARCA4 as a catalytic subunit, while it does  
498 not tolerate the incorporation of SMARCA2.

499 In summary, the IP-MS allowed us to characterize a novel configuration of the BAF complex (ARID1B-BAF),  
500 which is active during early stages of cranial neural crest differentiation and includes ARID1B, SMARCA4,  
501 and eight additional BAF subunits (Fig. 6e). Intriguingly, the transcription factor SALL4 also coeluted with  
502 ARID1B, suggesting a possible interaction with the complex, which was further supported by co-IP  
503 (Supplementary Fig. 3). Like ARID1B, SALL4 is also dispensable for the maintenance of the pluripotency  
504 networks, while it is essential for lineage commitment in early mammalian development, during which it  
505 targets sites with binding motifs also recognized by SOX2, OCT4 and NANOG<sup>22-25</sup>. SALL4 was previously  
506 shown to interact with the NuRD repressive complex<sup>23</sup>, while interactions with BAF have been largely  
507 unexplored. It was recently demonstrated that this transcription factor has affinity for AT-rich regions<sup>48</sup>,  
508 thus providing further support to the ARID1B-SALL4 interaction. *SALL4* mutations are also associated with  
509 developmental syndromes, including Okhiro syndrome, Holt-Oram syndrome, and Townes-Brocks  
510 Syndrome<sup>49</sup>. Notably, the *SALL4* gene is downregulated in the Coffin-Siris patients at CNCC day-5 but not  
511 in undifferentiated iPSCs, suggesting a possible feedback mechanism between *ARID1B* and *SALL4* during  
512 lineage commitment. Future studies will be necessary to support the speculation that SALL4 serves as an  
513 mediator for ARID1B-BAF recruitment at the pluripotency enhancers.

514

## 515 Discussion

516 ARID1B is a member of the evolutionarily conserved SWI/SNF (BAF) chromatin remodeler<sup>26,50</sup>. *De novo*  
517 haploinsufficient mutations in the *ARID1B* gene cause severe neurodevelopmental disorders which affect  
518 both physical and cognitive development.

519 In this study, we investigated the Coffin-Siris-associated *ARID1B* mutations in the context of craniofacial  
520 development and report the discovery of a novel function of the BAF complex: attenuation of the gene  
521 expression program associated with pluripotency maintenance upon differentiation cues. We found that  
522 this repressive function is performed at pluripotency enhancers and promoters by a specific and novel  
523 BAF complex configuration (ARID1B-BAF), which is composed of 10 subunits, with the enzymatic activity  
524 seemingly carried out exclusively by SMARCA4.

525 As a consequence of the *ARID1B* mutations, the Coffin-Siris patient cells fail to repress the pluripotency  
526 elements. This elicits aberrant SOX2 activity genome-wide, which in turn leads to the upregulation of  
527 multiple pluripotency genes, including *NANOG* and its associated gene network, and to the  
528 downregulation of the genes responsible for coordinating the exit from pluripotency  
529 (*PPAR $\alpha$* /*RXR $\alpha$*  pathway). We demonstrate that these pluripotency enhancers are normally maintained in  
530 an active state by ARID1A-BAF at the iPSC stage, and subsequently repressed by the ARID1B-BAF at the  
531 onset of cranial neural crest differentiation.

532 A switch between ARID1A-BAF and ARID1B-BAF upon differentiation cues is hence necessary for  
533 commitment towards the neural crest lineage.

534 Other studies have previously suggested that switches between SWI/SNF subunits play important roles in  
535 cell fate determination. For example, a switch between the two catalytic subunits SMARCA4 and  
536 SMARCA2 mediates the activation of human IFN $\gamma$ -activated genes<sup>51</sup>. Similarly, a gain of the subunit  
537 BAF53a in the neuron-specific BAF (nBAF) is required to control cell cycle exit in the developing neurons<sup>2,3</sup>.

538 With our study, we discovered a novel switch between BAF subunits (ARID1A/ARID1B), critical for the exit  
539 from pluripotency. Importantly, a balance between pro-self-renewal and pro-differentiation signals is  
540 pivotal for the determination of stem cell fate<sup>52</sup>. We demonstrate that such balance is lost in Coffin-Siris  
541 patients, whose cells are unable to perform the ARID1A/ARID1B switch at the pluripotency enhancers at  
542 the onset of differentiation. This switch is essential to successfully complete the cranial neural crest  
543 differentiation.

544 Pluripotency is orchestrated by a transcription factor network that needs to be extinguished in an orderly  
545 manner to enable lineage commitment and differentiation<sup>52-54</sup>. We find that ARID1B-BAF plays an  
546 essential role in this process, by means of a repressive activity at the pluripotency enhancers of the SOX2  
547 and NANOG networks. Similarly, an association between SOX3 and the SMARCA2 ATPase subunit of BAF  
548 was recently suggested in a study of neural development in the Nicolaides-Baraitser syndrome<sup>55</sup>. It is  
549 worth noting that Coffin-Siris and Nicolaides-Baraitser syndromes share many physical and neurological  
550 phenotypes<sup>55-57</sup>.

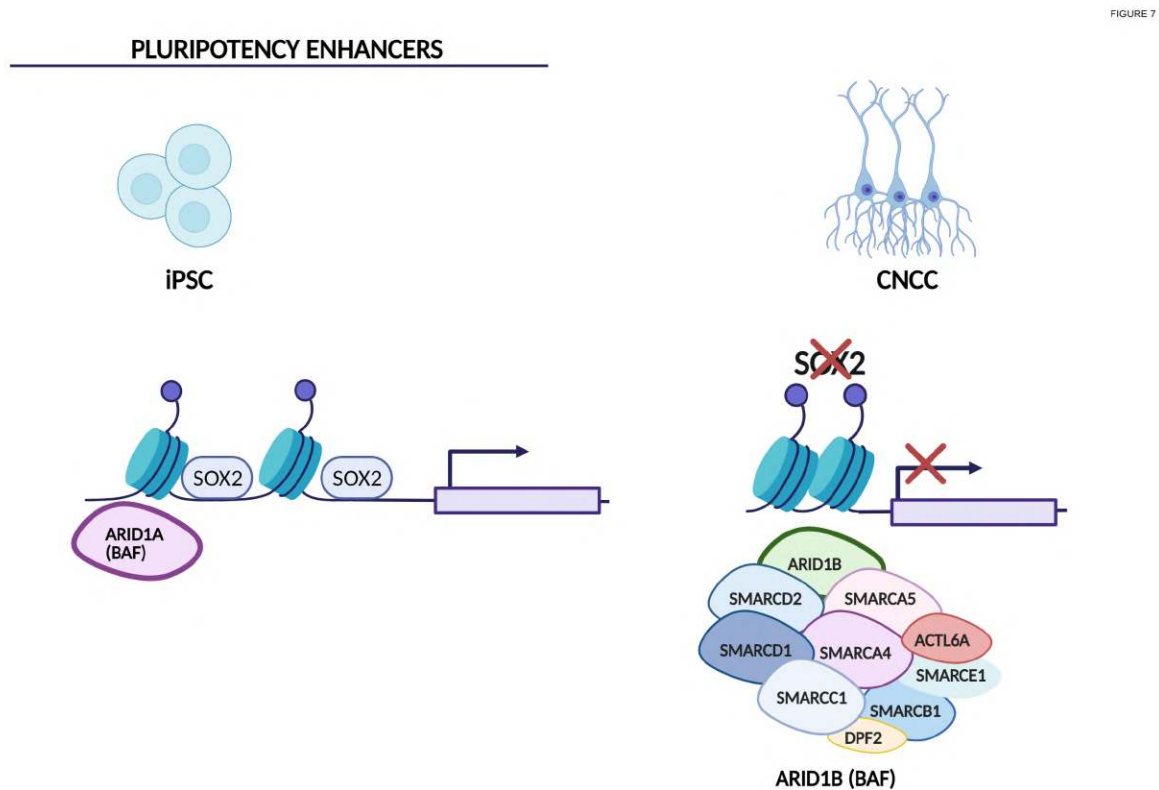
551 The BAF complex is predominantly considered as a transcriptional activator, which balances out the  
552 Polycomb Repressor Complexes (PRC1, PRC2) in the modulation of gene expression<sup>7,58</sup>. Nonetheless,  
553 repressing activity for BAF was also reported. For instance, a study conducted on hepatocellular  
554 carcinoma cell lines uncovered that ARID1A-containing BAF activates and represses roughly equal  
555 numbers of genes, while ARID1B-containing BAF was found to primarily repress enhancer activity<sup>47</sup>. Our  
556 experiments corroborate these findings, supporting an enhancer-repressor function for ARID1B-BAF. We  
557 demonstrate that the repressive activity of ARID1B-BAF is specific to a set of ~4,900 enhancers and ~600  
558 promoters, enriched for the SOX2 and NANOG binding sites. In *ARID1B*-wt conditions, these cis-regulatory  
559 elements are highly active at the iPSC stage, moderately active in the first four days of neural crest  
560 differentiation, and finally repressed by the day-5, a time point in which we reported the peak of ARID1B  
561 protein expression. The patient cells exhibit aberrant chromatin accessibility at these cis-regulatory  
562 elements for many days after the onset of differentiation, enforcing a long-lasting pluripotency signature  
563 which persists even after two weeks of differentiation.

564 Patient-26 derived cells display the most extreme cellular and molecular phenotype, with ~20% of the  
565 cells remaining pluripotent at the day-14 of differentiation, likely as a consequence of higher *SOX2* and  
566 *NANOG* expression and activity. The cells derived from this patient also show the highest levels of ARID1A  
567 binding at these enhancers at the day-5 of CNCC differentiation. Although it is difficult to formally  
568 compare disease severity since there are no accepted severity scales for Coffin-Siris syndrome, it is worth  
569 noting that Patient-26 presents clinically more severe than Patient-19. For example, Patient-26 was not  
570 able to speak at 7 years, whilst Patient-19 started speaking at 4 years. Additionally, the Patient-26 is  
571 affected by pyloric stenosis, a congenital anomaly in the digestive system thought to be associated with  
572 impaired migration of the enteric neural crest. We consider it unlikely that the difference is caused solely  
573 by the mutations in *ARID1B*, since both patients show comparable reduction in ARID1B protein levels. We  
574 speculate that additional genetic factors may concur with *ARID1B* haploinsufficiency to determine the  
575 clinical severity of the syndrome. Nonetheless, these lines of evidence potentially establish a direct  
576 correlation between reduced attenuation of pluripotency enhancers, inefficient exit from pluripotency,  
577 impaired cell differentiation, and disease severity (Fig. 7). However, additional experiments with a larger  
578 set of patient-derived cell lines would be required to support this model. Furthermore, it would also be  
579 important to investigate other differentiation lineages to elucidate whether the ARID1A/ARID1B switch is  
580 limited to the neural crest differentiation or if instead it represents a more widespread mechanism utilized  
581 by stem cells to exit the pluripotent state and undergo lineage commitment.

582 Finally, further investigations will be necessary to elucidate the mechanism(s) responsible for the  
583 repressive activity of ARID1B-BAF. Recent studies have demonstrated that the function of BAF (including  
584 ARID1A-BAF) as transcriptional activator is mediated by the AP-1 transcription factors<sup>55,59,60</sup>. On the other  
585 hand, little is known of potential co-factors mediating the repressive function of ARID1B-BAF. The



586 hypothesis that SALL4 might be mediating such repressive activity is fascinating and it opens up new  
587 research directions.  
588



589  
590  
591 **Figure 7 – A novel role for the ARID1B-BAF in the regulation of the exit from pluripotency.** In iPSCs, the  
592 pluripotency enhancers are maintained in active state by the ARID1A-BAF. When the neural crest  
593 differentiation is induced, ARID1B-BAF replaces ARID1A-BAF at these enhancers, eliciting their  
594 attenuation. The *ARID1B* haploinsufficient cells fail to perform the ARID1A/ARID1B switch, and maintain  
595 ARID1A-BAF at the pluripotency enhancers throughout the differentiation. Consequently, these  
596 enhancers remain aberrantly active and bound by SOX2 and NANOG for several days along the  
597 differentiation process. As a consequence, the gene network responsible for the exit from pluripotency  
598 is not efficiently activated and the CNCC differentiation is impaired.  
599

#### 600 **Acknowledgements**

601 The authors are deeply grateful to the patients and their families, who donated the samples for this  
602 research. The authors thank the physicians and technicians who collected and cultured the skin  
603 samples. This work was funded by the G. Harold and Leila Y. Mathers Foundation (MT), and the Gisela  
604 Thier Fellowship (GWES). The authors thank the Genomic Facilities at Thomas Jefferson University and at  
605 the Wistar Institute for the sequencing effort. The authors are grateful to Kelly Vonk (Leiden University)  
606 for the help with experimental procedures in the iPSC generation. An invaluable support was provided to  
607 the authors by the Stem Cell and Regenerative Neuroscience Center at Thomas Jefferson University, and  
608 in particular by Dr. Elizabeth Kropf. Lastly, MT and GWES are thankful to Dr. Samantha Vergano (Children's  
609 Hospital of the King Daughters) for making this collaboration and this work possible.  
610

611 **Author contributions:** MT, GWES and LP designed the project. GWES recruited the patients and obtained  
612 the skin fibroblasts. HMMM and CF reprogrammed the patient fibroblasts into iPSCs and assessed their  
613 quality. LD performed initial iPSC characterization experiments. LP performed most of the experiments.  
614 PP, ATC, CAO, and SAW contributed to specific experiments (flowcytometry, immunoblots, mass-  
615 spectrometry). BC provided intellectual contribution and financial support to PP. MT, LP and SD analyzed  
616 the data. MT, GWES, and LP wrote the manuscript, which was read and approved by all the authors.

617 **Data availability:** The original genome-wide data generate for this paper are deposited in the GEO  
618 database (accession number GSE169654).

619

## 620 **MATERIALS AND METHODS**

621

### 622 **Human iPSC culture**

623 Control iPSC lines were obtained from the iPSC Core of the University of Pennsylvania (Control line-1: SV20  
624 line, male, age 43) and from the Coriell Institute for Medical Research (Camden, NJ. Control line-2:  
625 GM23716, female, age 16).

626 Skin fibroblasts from the two pediatric Coffin-Siris patients (one teenager one young adult) were obtained  
627 by the team of Dr. Gijs Santen at Leiden University. Patient 19 is a female, while Patient 26 is a male. The  
628 fibroblasts were reprogrammed into iPSCs with the polycistronic lentiviral vector  
629 LV.RRL.PPT.SF.hOKSM.idTomato.-preFRT by LUMC human iPSC Hotel as described elsewhere<sup>61,62</sup>.

630 Multiple clones per line were derived. For each clone, pluripotency was assessed by immunofluorescence  
631 microscopy using antibodies against NANOG, OCT3/4, SSEA4 and Tra-1-81 under maintenance conditions  
632 and antibodies against (TUBB3, AFP and CD31) after spontaneous differentiation into the 3 germ layers as  
633 described elsewhere<sup>61</sup>. Clones with proper pluripotent characteristics were selected for downstream  
634 usage. Karyotyping by G binding was assessed for all the four lines by the Leiden University Medical Center  
635 and Short Tandem Repeat (STR) profiling was performed by the Leiden University Medical Center and and  
636 then replicated by the Stem Cell and Regenerative Neuroscience Center at Thomas Jefferson University.  
637 The iPSC lines were expanded in feeder-free, serum-free mTeSR<sup>TM</sup>1 medium (STEMCELL Technologies).  
638 Cells were passaged ~1:10 at 80% confluency using ReLeSR (STEMCELL Technologies) and small cell  
639 clusters (50–200 cells) were subsequently plated on tissue culture dishes coated overnight with Geltrex<sup>TM</sup>  
640 LDEV-Free hESC-qualified Reduced Growth Factor Basement Membrane Matrix (Fisher-Scientific).

641

### 642 **CNCC Differentiation**

643 The iPSC lines were differentiated into CNCC as previously described<sup>28</sup>. Briefly, iPSCs were treated with  
644 CNCC Derivation media: 1:1 Neurobasal medium/D-MEM F-12 medium (Invitrogen), 0.5× B-27  
645 supplement with Vitamin A (50× stock, Invitrogen), 0.5× N-2 supplement (100× stock, Invitrogen), 20  
646 ng/ml bFGF (Biolegend), 20 ng/ml EGF (Sigma-Aldrich), 5 µg/ml bovine insulin (Sigma-Aldrich) and 1×  
647 Glutamax-I supplement (100× stock, Invitrogen). Medium (3ml) was changed every day. Three days after  
648 the appearance of the migratory CNCC, cells were detached using accutase and placed into geltrex-coated  
649 plates. The early migratory CNCCs were then transitioned to CNCC early maintenance media: 1:1  
650 Neurobasal medium/D-MEM F-12 medium (Invitrogen), 0.5× B-27 supplement with Vitamin A (50× stock,  
651 Invitrogen), 0.5× N-2 supplement (100× stock, Invitrogen), 20 ng/ml bFGF (Biolegend), 20 ng/ml EGF  
652 (Sigma-Aldrich), 1 mg/ml bovine serum albumin, serum replacement grade (Gemini Bio-Products # 700-  
653 104P) and 1× Glutamax-I supplement (100× stock, Invitrogen).

654

655

### 656 **ARID1B Knock-down**

657 To make concentrated lentivirus, HEK293T cells were transfected with a pLenti plasmid in which we cloned  
658 an shRNA for *ARID1B* (GPP Web Portal: TRCN0000107361). iPSCs were lentivirally transduced by  
659 incubating the cells with concentrated virus overnight at 37 C. The next morning the media was changed,  
660 and 2 mg/ml puromycin (InvivoGen) were added 24h after infection. After 72 hours, the iPSCs that  
661 survived the selection were then differentiated in CNCC using the above described protocol, and collected  
662 at Day-5 for the genomic experiments. The cells were kept under puromycin selection for the entire  
663 duration of the differentiation. The knock-down efficiency was quantified via western blot.  
664

#### 665 **Flow cytometry analysis of surface markers**

666 To obtain a single cell suspension for flow cytometry analysis, control and patient cells were treated with  
667 Accutase for 5 minutes. Cells were then washed with cold PBS-2% FBS and live cells were counted.  $1 \times 10^6$   
668 cells/condition were resuspended in 100  $\mu$ L PBS-2% FBS and stained. For pluripotency evaluation, 4  $\mu$ L of  
669 the respective antibodies were used: APC anti-human SSEA-4 antibody (Biolegend, #330417) and PE anti-  
670 human TRA-1-60-R antibody (Biolegend, #330609). For analysis of differentiation, 2  $\mu$ L of the respective  
671 antibodies were used: FITC anti-human CD10 (Miltenyi Biotec, #130-124-262) and APC anti-human CD99  
672 (Miltenyi Biotec, #130-121-096). Cells were incubated for 15 min on ice and protected from light, before  
673 transferring them into FACS tubes containing additional 300  $\mu$ L PBS-2% FBS. Flow cytometry data were  
674 acquired using a BD LSR II flow cytometer and analyzed with FlowJo Software version 10.7.  
675

#### 676 **Western Blot**

677 For total lysate, cells were harvested and washed three times in 1X PBS and lysed in RIPA buffer (50mM  
678 Tris-HCl pH7.5, 150mM NaCl, 1% Igepal, 0.5% sodium deoxycholate, 0.1% SDS, 500uM DTT) with proteases  
679 inhibitors. Twenty  $\mu$ g of whole cell lysate were loaded in Novex WedgeWell 4-20% Tris-Glycine Gel  
680 (Invitrogen) and separated through gel electrophoresis (SDS-PAGE) Tris-Glycine-SDS buffer (Invitrogen).  
681 The proteins were then transferred to ImmunBlot PVDF membranes (ThermoFisher) for antibody probing.  
682 Membranes were incubated with 10% BSA in TBST for 30 minutes at room temperature (RT), then  
683 incubated for variable times with the suitable antibodies diluted in 5% BSA in 1X TBST, washed with TBST  
684 and incubated with a dilution of 1:10000 of secondary antibody for one hour at RT. The antibody was then  
685 visualized using Super Signal West Dura Extended Duration Substrat (ThermoFisher) and imaged with  
686 Amersham Imager 680.  
687

#### 688 **Cell fractionation**

689  $5 \times 10^6$  cells/condition were collected and suspended in E1 buffer (50mM HEPES-KOH, 140mM NaCl, 1mM  
690 EDTA, 10% glycerol, 0.5% NP-40, 0.25% Triton X-100, 1mM DTT, 1X Proteinase Inhibitor) followed by a  
691 centrifugation step of 1100 g at 4°C for 2min. The cytoplasmic fraction was collected in a fresh tube. Cells  
692 were washed two more times with E1 buffer. Pellet was subsequently suspended in E2 buffer (10mM Tris-  
693 HCl, 200mM NaCl, 1mM EDTA, 0.5mM EGTA, 1X Proteinase Inhibitor) followed by a centrifugation step of  
694 1100 g at 4°C for 2 min. Nuclear fraction was collected in a fresh tube. Cells were washed two more times  
695 with E2 buffer. After the third wash, pellet was suspended in E3 buffer (500mM Tris-HCl, 500mM NaCl, 1X  
696 Proteinase Inhibitor) and sonicated for 15 sec (5 sec ON/ 5 sec OFF). Cytoplasmic, nuclear and chromatin  
697 fraction were centrifuge at 16000 g for 10min at 4°C.  
698

#### 699 **Antibodies**

700 ARID1B ChIP-Seq: Abcam ab57461. ARID1B western blot: Santa-Cruz sc-32762 and Abcam ab57461.  
701 ARID1A ChIP-Seq: GeneTex GTX129433. ARID1A western blot: Cell Signaling Technologies 12354S. Beta-  
702 Actin western blot: Cell Signaling Technologies 8457P. SOX2 ChIP-Seq: Active Motif 39843. NANOG ChIP-  
703 Seq: R&D Systems AF1997. H3K27ac ChIP-Seq: Abcam ab4729. GAPDH western blot: Cell Signaling  
704 Technologies 5174T. CD10 Flow Cytometry: Miltenyi Biotec 130-124-262. CD99 Flow Cytometry: Miltenyi

705 Biotech 130-121-086. SSEA4 Flow Cytometry: Biologend 330417. TRA-1-60-R Flow Cytometry: Biologend  
706 330609. IgG ChIP-qPCR: Cell Signaling Technologies 2729S. Cell Signaling HRP-conjugated anti-rabbit  
707 (7074S) and anti-mouse (7076S) were used as secondary antibodies in western blot. Spike-in Antibody:  
708 Active Motif 61686. Spike-in Chromatin: Active Motif 53083.

709

#### 710 **Real-time quantitative polymerase chain reaction (RT-qPCR)**

711 Cells were lysed in Tri-reagent and RNA was extracted using the Direct-zol RNA MiniPrep kit (Zymo  
712 research). 600ng of template RNA was retrotranscribed into cDNA using RevertAid first strand cDNA  
713 synthesis kit (Thermo Scientific) according to manufacturer directions. 15ng of cDNA were used for each  
714 real-time quantitative PCR reaction with 0.1  $\mu$ M of each primer, 10  $\mu$ L of PowerUp™ SYBR™ Green Master  
715 Mix (Applied Biosystems) in a final volume of 20  $\mu$ L, using QuantStudio 3 Real-Time PCR System (Applied  
716 Biosystem). Thermal cycling parameters were set as following: 3 minutes at 95°C, followed by 40 cycles of  
717 10 s at 95°C, 20 s at 63°C followed by 30 s at 72°C. Each sample was run in triplicate. 18S rRNA was used  
718 as normalizer. Primer sequences are reported in Supplementary Table S1.

719

#### 720 **ChIP-Seq and ChIP-qPCR**

721 Samples from different conditions were processed together to prevent batch effects.

722 For SOX2, NANOG and H3K27ac, for each replicate, 10 million cells were cross-linked with 1%  
723 formaldehyde for 5 min at room temperature, quenched with 125mM glycine, harvested and washed  
724 twice with 1 $\times$  PBS. The pellet was resuspended in ChIP lysis buffer (150 mM NaCl, 1% Triton X-100, 0.7%  
725 SDS, 500  $\mu$ M DTT, 10 mM Tris-HCl, 5 mM EDTA) and chromatin was sheared to an average length of 200–  
726 500 bp, using a Covaris S220 Ultrasonicator. The chromatin lysate was diluted with SDS-free ChIP lysis  
727 buffer. For ChIP-seq, 10  $\mu$ g of antibody (3  $\mu$ g for H3K27ac) was added to 5  $\mu$ g of sonicated chromatin along  
728 with Dynabeads Protein A magnetic beads (Invitrogen) and incubated at 4 °C overnight. For SOX2 and  
729 NANOG ChIP-seq, 10 ng of spike-in Drosophila chromatin (Active Motif) was added to each sample with  
730 2  $\mu$ g spike-in antibody (Active Motif). On day 2, beads were washed twice with each of the following  
731 buffers: Mixed Micelle Buffer (150 mM NaCl, 1% Triton X-100, 0.2% SDS, 20 mM Tris-HCl, 5 mM EDTA,  
732 65% sucrose), Buffer 500 (500 mM NaCl, 1% Triton X-100, 0.1% Na deoxycholate, 25 mM HEPES, 10 mM  
733 Tris-HCl, 1 mM EDTA), LiCl/detergent wash (250 mM LiCl, 0.5% Na deoxycholate, 0.5% NP-40, 10 mM Tris-  
734 HCl, 1 mM EDTA) and a final wash was performed with 1 $\times$  TE. Finally, beads were resuspended in 1 $\times$  TE  
735 containing 1% SDS and incubated at 65 °C for 10 min to elute immunocomplexes. Elution was repeated  
736 twice, and the samples were further incubated overnight at 65 °C to reverse cross-linking, along with the  
737 untreated input (5% of the starting material). On day 3, after treatment with 0.5 mg/ml Proteinase K for  
738 1h at 65 °C, DNA was purified with Zymo ChIP DNA Clear Concentrator kit and quantified with QUBIT.

739 For ARID1A and ARID1B ChIP-Seq, 10 million cells were cross-linked with EGS (150 mM) for 30min at room  
740 temperature followed by a second cross-link with 1% formaldehyde for 15 min at room temperature. The  
741 formaldehyde was quenched with by adding glycine (0.125M) for 10 min at room temperature. Cells were  
742 washed twice with 1 $\times$  PBS. Pellet was resuspended in buffer LB1 (50 mM Hepes-KOH, 140 mM NaCl, 1 mM  
743 EDTA, 10% Glycerol, 0.5% NP-40, 0.255 Triton X-100), incubated 10 min at 4 °C followed by a  
744 centrifugation step of 600g for 5 min at 4 °C. Pellet was suspended in buffer LB2 (10 mM Tris-HCl, 20 mM  
745 NaCl, 1 mM EDTA, 0.5 mM EGTA) incubated 10 min at 4 °C followed by a centrifugation step of 600g for 5  
746 min at 4 °C. Cells were then resuspended in buffer LB3 (10 mM Tris-HCl, 200 mM NaCl, 1mM EDTA, 0.5  
747 mM EGTA, 0.1% Na-DOC, 0.5% N-lauroylsarcosine) incubated 10 min at 4 °C followed by a centrifugation  
748 step of 600g for 5min at 4 °C. Pellet was suspended in LB3 and chromatin was sheared to an average  
749 length of 200–500 bp, using a Covaris S220 Ultrasonicator. For each sample, 15  $\mu$ g of sonicated chromatin  
750 was incubated at 4 °C overnight along with Dynabeads Protein G conjugated with 10 $\mu$ g of antibody. On  
751 day 2, beads were washed once with each of the following buffers: WB1 (50 mM Tris-HCl, 150 mM NaCl,  
752 0.15 SDS, 0.1% Na-DOC, 1% Triton X-100, 1 mM EDTA), WB2 (50 mM Tris-HCl, 500 mM NaCl, 0.15 SDS,



753 0.1% Na-DOC, 1% Triton X-100, 1 mM EDTA), WB3 (10 mM Tris-HCl, 250 mM LiCl, 0.55 NP-40, 0.55 Na-  
754 DOC, 1 mM EDTA), TE Buffer (10 mM Tris-HCl, 1mM EDTA). Finally, beads were resuspended in EB (10 mM  
755 tris-HCl, 0.55 SDS, 300 mM NaCl, 5mM EDTA) and incubated at 65 °C for 30 min to elute  
756 immunocomplexes. Elution was repeated twice, and the samples were further incubated overnight at 65  
757 °C to reverse cross-linking, along with the untreated input (5% of the starting material). On day 3, after  
758 treatment with 0.5 mg/ml Proteinase K for 1h at 65 °C.

759 For all ChIP-seq experiments, barcoded libraries were made with NEB ULTRA II DNA Library Prep Kit for  
760 Illumina, and sequenced on Illumina NextSeq 500, producing 75bp SE reads.

761 For ChIP-qPCR, on day 1 the sonicated lysate was aliquot into single immunoprecipitations of  $2.5 \times 10^6$   
762 cells each. A specific antibody or a total rabbit IgG control was added to the lysate along with Protein A  
763 magnetic beads (Invitrogen) and incubated at 4 °C overnight. On day3, ChIP eluates and input were  
764 assayed by real-time quantitative PCR in a 20 µl reaction with the following: 0.4 µM of each primer, 10 µl  
765 of PowerUp SYBR Green (Applied Biosystems), and 5 µl of template DNA (corresponding to 1/40 of the  
766 elution material) using the fast program on QuantStudio qPCR machine (Applied Biosystems). Thermal  
767 cycling parameters were: 20sec at 95 °C, followed by 40 cycles of 1sec at 95°C, 20sec at 60°C.

768

### 769 **ChIP-seq Analyses**

770 After removing the adapters, the sequences were aligned to the reference hg19, using Burrows Wheeler  
771 Alignment tool (BWA), with the MEM algorithm<sup>63</sup>. Aligned reads were filtered based on mapping quality  
772 (MAPQ > 10) to restrict our analysis to higher quality and likely uniquely mapped reads, and PCR duplicates  
773 were removed. We called peaks for each individual using MACS2<sup>64</sup> (H3K27ac) or Homer<sup>65</sup>, at 5% FDR, with  
774 default parameters.

775

### 776 **RNA-Seq**

777 Cells were lysed in Tri-reagent (Zymo research) and total RNA was extracted using Quick-RNA Miniprep  
778 kit (Zymo research) according to the manufacturer's instructions. RNA was further quantified using  
779 DeNovix DS-11 Spectrophotometer while the RNA integrity was checked on Bioanalyzer 2100 (Agilent).  
780 Only samples with RIN value above 8.0 were used for transcriptome analysis. RNA libraries were prepared  
781 using 1 µg of total RNA input using NEBNext<sup>®</sup> Poly(A) mRNA Magnetic Isolation Module, NEBNext<sup>®</sup>  
782 UltraTM II Directional RNA Library Prep Kit for Illumina<sup>®</sup> and NEBNext<sup>®</sup> UltraTM II DNA Library Prep Kit for  
783 Illumina<sup>®</sup> according to the manufacturer's instructions (New England Biolabs).

784

### 785 **RNA-Seq Analyses**

786 Reads were aligned to hg19 using STAR v2.5<sup>66</sup>, in 2-pass mode with the following parameters: --  
787 quantMode TranscriptomeSAM --outFilterMultimapNmax 10 - -outFilterMismatchNmax 10 --  
788 outFilterMismatchNoverLmax 0.3 --alignIntronMin 21 -- alignIntronMax 0 --alignMatesGapMax 0 --  
789 alignSJoverhangMin 5 --runThreadN 12 -- twopassMode Basic --twopass1readsN 60000000 --  
790 sjdbOverhang 100. We filtered bam files based on alignment quality (q = 10) using Samtools v0.1.19<sup>63</sup>. We  
791 used the latest annotations obtained from Ensembl to build reference indexes for the STAR alignment.  
792 Kallisto<sup>67</sup> was used to count reads mapping to each gene. RSEM<sup>68</sup> was instead used to obtain FPKM  
793 (Fragments Per Kilobase of exon per Million fragments mapped). We analyzed differential gene expression  
794 levels with DESeq2<sup>69</sup>, with the following model: design = ~condition, where condition indicates either CTRL  
795 or Patients.

796

### 797 **ATAC-Seq**

798 For ATAC-Seq experiments, 50,000 cells per condition were processed as described in the original ATAC-  
799 seq protocol paper<sup>70</sup>. ATAC-seq data were processed with the same pipeline described for ChIP-seq, with  
800 one modification: all mapped reads were offset by +4 bp for the forward-strand and -5 bp for the reverse-

801 strand. After peak calling (MACS2), peaks replicated in all 4 lines (hereafter consensus peaks) were used  
802 for downstream analyses.

803

#### 804 **Nuclear extract, IP and LC-MS/MS**

805 After collection, cells were washed twice with ice cold PBS before resuspension in co-IP buffer (20mM Tris  
806 pH 7.9, 100mM NaCl, 0.1% NP-40, 0.5mM DTT, protease inhibitors), and rotated for 5 minutes at 4°C.  
807 After spinning down at 2000rpm for 10 minutes, the nuclear pellet was resuspended in buffer C (20mM  
808 Tris pH 8.0, 1.5mM MgCl<sub>2</sub>, 0.42M NaCl, 25% glycerol, 0.2mM EDTA, 0.5mM DTT, protease inhibitors),  
809 dounce homogenized (with B pestle), and incubated at 4°C for 30 minutes. The extract was centrifuged at  
810 12,000rpm for 30 minutes, and the supernatant was kept as nuclear extract. The nuclear extract was  
811 dialyzed overnight in BC80 (20mM Tris pH 8.0, 80mM KCl, 0.2mM EDTA, 10% glycerol, 1mM B-  
812 mercaptoethanol, 0.2mM phenylmethylsulfonyl fluoride (PMSF)), cleared, and stored at -80°C. For the IP,  
813 1.5mg of nuclear extract was incubated for 3 hours at 4°C with 6µg ARID1B antibody and 50µL of  
814 Dynabeads Protein A, and the control IP was performed with 0.75mg of nuclear extract and 25µL of  
815 Dynabeads Protein A. Beads were washed three times with co-IP buffer, followed by a final wash with  
816 0.05% NP-40 in PBS. Elution was performed by agitation in 0.1M glycine pH 3.0 for one minute, and 1M  
817 Tris base pH 11.0 was added to neutralize the pH of the eluate. Eluates were prepared for SDS-PAGE and  
818 run on a Novex WedgeWell 10% Tris-Glycine Gel (Invitrogen) with Tris-Glycine-SDS buffer (Bio-Rad), at  
819 110V for 10 minutes. The gel was stained with Colloidal Blue staining kit (Invitrogen), and further  
820 processed at the proteomics facility at the Wistar Institute. Briefly, the gel lanes were excised, reduced  
821 with TCEP, alkylated with iodoacetamide, and digested with trypsin. Tryptic digests were analyzed using  
822 LC-MS/MS (a standard 90 minute LC gradient on the Thermo Q Exactive HF mass spectrometer). MS/MS  
823 spectra were searched with full tryptic specificity against the UniProt human database (10/02/2020) using  
824 MaxQuant 1.6.17.0, and also searched for the common protein N-terminal acetylation, Asn deamidation,  
825 and Met oxidation. Protein and peptide false discovery rate was set at 1%.

826

#### 827 **Statistical and genomic analyses**

828 All statistical analyses were performed using R v3.3.1. BEDtools v2.27.1<sup>71</sup> was used for genomic analyses.  
829 Pathway analysis was performed with Ingenuity Pathway Analysis Suite (QIAGEN Inc.,  
830 <https://www.qiagenbioinformatics.com/products/ingenuity-pathway-analysis>). Motif analyses were  
831 performed using the Meme-Suite<sup>72</sup>, and specifically with the Meme-ChIP application. Fasta files of the  
832 regions of interest were produced using BEDTools v2.27.1. Shuffled input sequences were used as  
833 background. E-values < 0.001 were used as threshold for significance<sup>72</sup>.

834

835

#### 836 **References**

- 837 1. Wang, W. *et al.* Purification and biochemical heterogeneity of the mammalian SWI-SNF  
838 complex. *EMBO J* **15**, 5370-82 (1996).
- 839 2. Braun, S.M.G. *et al.* BAF subunit switching regulates chromatin accessibility to control cell  
840 cycle exit in the developing mammalian cortex. *Genes Dev* **35**, 335-353 (2021).
- 841 3. Lessard, J. *et al.* An essential switch in subunit composition of a chromatin remodeling  
842 complex during neural development. *Neuron* **55**, 201-15 (2007).
- 843 4. Gatchalian, J. *et al.* A non-canonical BRD9-containing BAF chromatin remodeling complex  
844 regulates naive pluripotency in mouse embryonic stem cells. *Nat Commun* **9**, 5139 (2018).

- 845 5. Ho, L. *et al.* An embryonic stem cell chromatin remodeling complex, esBAF, is an essential  
846 component of the core pluripotency transcriptional network. *Proc Natl Acad Sci U S A* **106**,  
847 5187-91 (2009).
- 848 6. Ho, L. *et al.* An embryonic stem cell chromatin remodeling complex, esBAF, is essential  
849 for embryonic stem cell self-renewal and pluripotency. *Proc Natl Acad Sci U S A* **106**, 5181-  
850 6 (2009).
- 851 7. Alfert, A., Moreno, N. & Kerl, K. The BAF complex in development and disease. *Epigenetics*  
852 *Chromatin* **12**, 19 (2019).
- 853 8. Halgren, C. *et al.* Corpus callosum abnormalities, intellectual disability, speech  
854 impairment, and autism in patients with haploinsufficiency of ARID1B. *Clin Genet* **82**, 248-  
855 55 (2012).
- 856 9. Hoyer, J. *et al.* Haploinsufficiency of ARID1B, a member of the SWI/SNF-a chromatin-  
857 remodeling complex, is a frequent cause of intellectual disability. *Am J Hum Genet* **90**,  
858 565-72 (2012).
- 859 10. Santen, G.W. *et al.* Mutations in SWI/SNF chromatin remodeling complex gene ARID1B  
860 cause Coffin-Siris syndrome. *Nat Genet* **44**, 379-80 (2012).
- 861 11. Tsurusaki, Y. *et al.* Coffin-Siris syndrome is a SWI/SNF complex disorder. *Clin Genet* **85**,  
862 548-54 (2014).
- 863 12. van der Sluijs, P.J. *et al.* The ARID1B spectrum in 143 patients: from nonsyndromic  
864 intellectual disability to Coffin-Siris syndrome. *Genet Med* **21**, 1295-1307 (2019).
- 865 13. Vergano, S.A., van der Sluijs, P.J. & Santen, G. ARID1B-Related Disorder. in  
866 *GeneReviews((R))* (eds. Adam, M.P. *et al.*) (Seattle (WA), 1993).
- 867 14. Santen, G.W. *et al.* Coffin-Siris syndrome and the BAF complex: genotype-phenotype  
868 study in 63 patients. *Hum Mutat* **34**, 1519-28 (2013).
- 869 15. Wiczorek, D. *et al.* A comprehensive molecular study on Coffin-Siris and Nicolaides-  
870 Baraitser syndromes identifies a broad molecular and clinical spectrum converging on  
871 altered chromatin remodeling. *Hum Mol Genet* **22**, 5121-35 (2013).
- 872 16. Wright, C.F. *et al.* Genetic diagnosis of developmental disorders in the DDD study: a  
873 scalable analysis of genome-wide research data. *Lancet* **385**, 1305-14 (2015).
- 874 17. Jung, E.M. *et al.* Arid1b haploinsufficiency disrupts cortical interneuron development and  
875 mouse behavior. *Nat Neurosci* **20**, 1694-1707 (2017).
- 876 18. Ka, M., Chopra, D.A., Dravid, S.M. & Kim, W.Y. Essential Roles for ARID1B in Dendritic  
877 Arborization and Spine Morphology of Developing Pyramidal Neurons. *J Neurosci* **36**,  
878 2723-42 (2016).
- 879 19. Shibutani, M. *et al.* Arid1b Haploinsufficiency Causes Abnormal Brain Gene Expression  
880 and Autism-Related Behaviors in Mice. *Int J Mol Sci* **18**(2017).
- 881 20. Smith, A.L., Jung, E.M., Jeon, B.T. & Kim, W.Y. Arid1b haploinsufficiency in parvalbumin-  
882 or somatostatin-expressing interneurons leads to distinct ASD-like and ID-like behavior.  
883 *Sci Rep* **10**, 7834 (2020).
- 884 21. Sausen, M. *et al.* Integrated genomic analyses identify ARID1A and ARID1B alterations in  
885 the childhood cancer neuroblastoma. *Nat Genet* **45**, 12-7 (2013).
- 886 22. Lu, J. *et al.* Stem cell factor SALL4 represses the transcriptions of PTEN and SALL1 through  
887 an epigenetic repressor complex. *PLoS One* **4**, e5577 (2009).

- 888 23. Miller, A. *et al.* Sall4 controls differentiation of pluripotent cells independently of the  
889 Nucleosome Remodelling and Deacetylation (NuRD) complex. *Development* **143**, 3074-84  
890 (2016).
- 891 24. Tatetsu, H. *et al.* SALL4, the missing link between stem cells, development and cancer.  
892 *Gene* **584**, 111-9 (2016).
- 893 25. Yang, J. *et al.* Genome-wide analysis reveals Sall4 to be a major regulator of pluripotency  
894 in murine-embryonic stem cells. *Proc Natl Acad Sci U S A* **105**, 19756-61 (2008).
- 895 26. Mashtalir, N. *et al.* Modular Organization and Assembly of SWI/SNF Family Chromatin  
896 Remodeling Complexes. *Cell* **175**, 1272-1288 e20 (2018).
- 897 27. Inoue, K. *et al.* Molecular mechanism for distinct neurological phenotypes conveyed by  
898 allelic truncating mutations. *Nat Genet* **36**, 361-9 (2004).
- 899 28. Prescott, S.L. *et al.* Enhancer divergence and cis-regulatory evolution in the human and  
900 chimp neural crest. *Cell* **163**, 68-83 (2015).
- 901 29. Liu, X. *et al.* De Novo ARID1B mutations cause growth delay associated with aberrant  
902 Wnt/beta-catenin signaling. *Hum Mutat* **41**, 1012-1024 (2020).
- 903 30. Vasileiou, G. *et al.* Chromatin-Remodeling-Factor ARID1B Represses Wnt/beta-Catenin  
904 Signaling. *Am J Hum Genet* **97**, 445-56 (2015).
- 905 31. Lee, J., Lee, J. & Cho, Y.S. Peroxisome Proliferator-Activated Receptor alpha Agonist and  
906 Its Target Nanog Cooperate to Induce Pluripotency. *J Clin Med* **7**(2018).
- 907 32. Mullen, E.M., Gu, P. & Cooney, A.J. Nuclear Receptors in Regulation of Mouse ES Cell  
908 Pluripotency and Differentiation. *PPAR Res* **2007**, 61563 (2007).
- 909 33. Rajasingh, J. & Bright, J.J. 15-Deoxy-delta12,14-prostaglandin J2 regulates leukemia  
910 inhibitory factor signaling through JAK-STAT pathway in mouse embryonic stem cells. *Exp*  
911 *Cell Res* **312**, 2538-46 (2006).
- 912 34. Dodonova, S.O., Zhu, F., Dienemann, C., Taipale, J. & Cramer, P. Nucleosome-bound SOX2  
913 and SOX11 structures elucidate pioneer factor function. *Nature* **580**, 669-672 (2020).
- 914 35. King, H.W. & Klose, R.J. The pioneer factor OCT4 requires the chromatin remodeller BRG1  
915 to support gene regulatory element function in mouse embryonic stem cells. *Elife*  
916 **6**(2017).
- 917 36. Blassberg, R. *et al.* Sox2 levels configure the WNT response of epiblast progenitors  
918 responsible for vertebrate body formation. 2020.12.29.424684 (2020).
- 919 37. Bunina, D. *et al.* Genomic Rewiring of SOX2 Chromatin Interaction Network during  
920 Differentiation of ESCs to Postmitotic Neurons. *Cell Syst* **10**, 480-494 e8 (2020).
- 921 38. Heurtier, V. *et al.* The molecular logic of Nanog-induced self-renewal in mouse embryonic  
922 stem cells. *Nat Commun* **10**, 1109 (2019).
- 923 39. Novo, C.L. *et al.* The pluripotency factor Nanog regulates pericentromeric  
924 heterochromatin organization in mouse embryonic stem cells. *Genes Dev* **30**, 1101-15  
925 (2016).
- 926 40. De Kumar, B. *et al.* Dynamic regulation of Nanog and stem cell-signaling pathways by  
927 Hoxa1 during early neuro-ectodermal differentiation of ES cells. *Proc Natl Acad Sci U S A*  
928 **114**, 5838-5845 (2017).
- 929 41. Navarro, P. *et al.* OCT4/SOX2-independent Nanog autorepression modulates  
930 heterogeneous Nanog gene expression in mouse ES cells. *EMBO J* **31**, 4547-62 (2012).



- 931 42. Silva, J. *et al.* Nanog is the gateway to the pluripotent ground state. *Cell* **138**, 722-37  
932 (2009).
- 933 43. Gagliardi, A. *et al.* A direct physical interaction between Nanog and Sox2 regulates  
934 embryonic stem cell self-renewal. *EMBO J* **32**, 2231-47 (2013).
- 935 44. Rodda, D.J. *et al.* Transcriptional regulation of nanog by OCT4 and SOX2. *J Biol Chem* **280**,  
936 24731-7 (2005).
- 937 45. Shang, L. *et al.* Mutations in ARID2 are associated with intellectual disabilities.  
938 *Neurogenetics* **16**, 307-14 (2015).
- 939 46. Trizzino, M. *et al.* The Tumor Suppressor ARID1A Controls Global Transcription via Pausing  
940 of RNA Polymerase II. *Cell Rep* **23**, 3933-3945 (2018).
- 941 47. Raab, J.R., Resnick, S. & Magnuson, T. Genome-Wide Transcriptional Regulation Mediated  
942 by Biochemically Distinct SWI/SNF Complexes. *PLoS Genet* **11**, e1005748 (2015).
- 943 48. Pantier, R. *et al.* SALL4 controls cell fate in response to DNA base composition. *Mol Cell*  
944 **81**, 845-858 e8 (2021).
- 945 49. Kohlhase, J. SALL4-Related Disorders. in *GeneReviews((R))* (eds. Adam, M.P. *et al.*) (Seattle  
946 (WA), 1993).
- 947 50. Pagliaroli, L. & Trizzino, M. The Evolutionary Conserved SWI/SNF Subunits ARID1A and  
948 ARID1B Are Key Modulators of Pluripotency and Cell-Fate Determination. *Front Cell Dev*  
949 *Biol* **9**, 643361 (2021).
- 950 51. Zhang, Y. *et al.* A switch from hBrm to Brg1 at IFN $\gamma$ -activated sequences mediates  
951 the activation of human genes. *Cell Res* **20**, 1345-60 (2010).
- 952 52. Betschinger, J. *et al.* Exit from pluripotency is gated by intracellular redistribution of the  
953 bHLH transcription factor Tfe3. *Cell* **153**, 335-47 (2013).
- 954 53. Jaenisch, R. & Young, R. Stem cells, the molecular circuitry of pluripotency and nuclear  
955 reprogramming. *Cell* **132**, 567-82 (2008).
- 956 54. Takahashi, K. & Yamanaka, S. A decade of transcription factor-mediated reprogramming  
957 to pluripotency. *Nat Rev Mol Cell Biol* **17**, 183-93 (2016).
- 958 55. Gao, F. *et al.* Heterozygous Mutations in SMARCA2 Reprogram the Enhancer Landscape  
959 by Global Retargeting of SMARCA4. *Mol Cell* **75**, 891-904 e7 (2019).
- 960 56. Ejaz, R., Babul-Hirji, R. & Chitayat, D. The evolving features of Nicolaides-Baraitser  
961 syndrome - a clinical report of a 20-year follow-up. *Clin Case Rep* **4**, 351-5 (2016).
- 962 57. Wolff, D. *et al.* In-Frame Deletion and Missense Mutations of the C-Terminal Helicase  
963 Domain of SMARCA2 in Three Patients with Nicolaides-Baraitser Syndrome. *Mol*  
964 *Syndromol* **2**, 237-244 (2012).
- 965 58. Kadoch, C. & Crabtree, G.R. Mammalian SWI/SNF chromatin remodeling complexes and  
966 cancer: Mechanistic insights gained from human genomics. *Sci Adv* **1**, e1500447 (2015).
- 967 59. Mathur, R. *et al.* ARID1A loss impairs enhancer-mediated gene regulation and drives colon  
968 cancer in mice. *Nat Genet* **49**, 296-302 (2017).
- 969 60. Vierbuchen, T. *et al.* AP-1 Transcription Factors and the BAF Complex Mediate Signal-  
970 Dependent Enhancer Selection. *Mol Cell* **68**, 1067-1082 e12 (2017).
- 971 61. Warlich, E. *et al.* Lentiviral vector design and imaging approaches to visualize the early  
972 stages of cellular reprogramming. *Mol Ther* **19**, 782-9 (2011).

- 973 62. Chen, J. *et al.* Rational optimization of reprogramming culture conditions for the  
974 generation of induced pluripotent stem cells with ultra-high efficiency and fast kinetics.  
975 *Cell Res* **21**, 884-94 (2011).
- 976 63. Li, H. *et al.* The Sequence Alignment/Map format and SAMtools. *Bioinformatics* **25**, 2078-  
977 9 (2009).
- 978 64. Zhang, Y. *et al.* Model-based analysis of ChIP-Seq (MACS). *Genome Biol* **9**, R137 (2008).
- 979 65. Heinz, S. *et al.* Simple combinations of lineage-determining transcription factors prime  
980 cis-regulatory elements required for macrophage and B cell identities. *Mol Cell* **38**, 576-  
981 89 (2010).
- 982 66. Dobin, A. *et al.* STAR: ultrafast universal RNA-seq aligner. *Bioinformatics* **29**, 15-21 (2013).
- 983 67. Bray, N.L., Pimentel, H., Melsted, P. & Pachter, L. Near-optimal probabilistic RNA-seq  
984 quantification. *Nat Biotechnol* **34**, 525-7 (2016).
- 985 68. Li, B. & Dewey, C.N. RSEM: accurate transcript quantification from RNA-Seq data with or  
986 without a reference genome. *BMC Bioinformatics* **12**, 323 (2011).
- 987 69. Love, M.I., Huber, W. & Anders, S. Moderated estimation of fold change and dispersion  
988 for RNA-seq data with DESeq2. *Genome Biol* **15**, 550 (2014).
- 989 70. Buenrostro, J.D., Giresi, P.G., Zaba, L.C., Chang, H.Y. & Greenleaf, W.J. Transposition of  
990 native chromatin for fast and sensitive epigenomic profiling of open chromatin, DNA-  
991 binding proteins and nucleosome position. *Nat Methods* **10**, 1213-8 (2013).
- 992 71. Quinlan, A.R. & Hall, I.M. BEDTools: a flexible suite of utilities for comparing genomic  
993 features. *Bioinformatics* **26**, 841-2 (2010).
- 994 72. Bailey, T.L. *et al.* MEME SUITE: tools for motif discovery and searching. *Nucleic Acids Res*  
995 **37**, W202-8 (2009).
- 996